

## On the future navigability of Arctic sea routes: High-resolution projections of the Arctic Ocean and sea ice



Yevgeny Aksenov<sup>a,\*</sup>, Ekaterina E. Popova<sup>a</sup>, Andrew Yool<sup>a</sup>, A.J. George Nurser<sup>a</sup>, Timothy D. Williams<sup>b</sup>, Laurent Bertino<sup>b</sup>, Jon Bergh<sup>b</sup>

<sup>a</sup> National Oceanography Centre, Southampton SO14 3ZH, UK

<sup>b</sup> Nansen Environmental and Remote Sensing Center, Bergen N-5006, Norway

### ARTICLE INFO

#### Article history:

Received 29 October 2015

Received in revised form

31 December 2015

Accepted 31 December 2015

Available online 4 February 2016

#### Keywords:

Arctic Ocean

Arctic shipping routes

CO<sub>2</sub> emission scenarios

Climate change projections

Sea ice

Marginal Ice Zone

Ocean waves

### ABSTRACT

The rapid Arctic summer sea ice reduction in the last decade has led to debates in the maritime industries on the possibility of an increase in cargo transportation in the region. Average sailing times on the North Sea Route along the Siberian Coast have fallen from 20 days in the 1990s to 11 days in 2012–2013, attributed to easing sea ice conditions along the Siberian coast. However, the economic risk of exploiting the Arctic shipping routes is substantial. Here a detailed high-resolution projection of ocean and sea ice to the end of the 21st century forced with the RCP8.5 IPCC emission scenario is used to examine navigability of the Arctic sea routes. In summer, opening of large areas of the Arctic Ocean previously covered by pack ice to the wind and surface waves leads to Arctic pack ice cover evolving into the Marginal Ice Zone. The emerging state of the Arctic Ocean features more fragmented thinner sea ice, stronger winds, ocean currents and waves. By the mid 21st century, summer season sailing times along the route via the North Pole are estimated to be 13–17 days, which could make this route as fast as the North Sea Route.

© 2016 The Authors. Published by Elsevier Ltd. This is an open access article under the CC BY license (<http://creativecommons.org/licenses/by/4.0/>).

### 1. Introduction

The United Nations Framework Convention on Climate Change (UNFCCC) held in Copenhagen in December 2009 agreed that global greenhouse emissions, including shipping, must be capped to prevent global temperature rising by more than 2 °C. This places heavy challenges on the industry. The estimated share of CO<sub>2</sub> emissions from shipping in the total global anthropogenic CO<sub>2</sub> emissions was about 3.3% in the 2000s [1]. Taking into account the projected increase in the volume of shipping, the emissions from global shipping operations will rise by 20–60% by 2050. To achieve the target global CO<sub>2</sub> concentration level of 450 ppm by 2050, global shipping is targeted to reduce its emissions at the rate of 2.6% per year from 2020 to 2050 [2–4]. The measures put in place by the International Maritime Organization (IMO) [5,6], including the recently adopted Energy Efficiency Design Index (EEDI), do not guarantee reaching the required reduction. Additional solutions must be sought, like switching to low-emission fuels, such as Liquid Natural Gas (LNG), hydrogen, biofuels, or non-emissive

propulsion, solar- and wind-powered [7], reducing the water drag of ship's hulls and reducing the speed of sailing for cargo vessels (slow steaming). These measures will require several years to implement, and will require refitting the existing fleet at a very large expense for industry [8,9].

The exploitation of shipping routes in the Arctic Ocean can, in principle, reduce the navigational distances between Europe and Asia by about 40%, saving fuel and reducing CO<sub>2</sub> emissions [10]. Schøyen and Bråthen analyzed a potential reduction in sailing time, fuel and CO<sub>2</sub> emission savings for two types of bulk cargo vessels sailing along the Northern Sea Route (NSR) instead of via the Suez Canal [10]. They concluded that the main advantage of shipping operations using an ice-free NSR would be the reduction of sailing time, more than doubling the fuel efficiency and reducing CO<sub>2</sub> emissions by 49–78%. They however asserted that this would not necessarily be the case for liner shipping due to uncertainty in the schedule reliability for the NSR so, in the short term, this route would first be of interest for bulk shipping. Overall, the saving in fuel might not necessarily translate to cost savings because of other factors, such as higher building costs for ice-classed ships, service irregularity and slower speeds, navigation difficulties, greater safety risks, etc., and, probably the most important factor, fees for icebreaker services. [10,11].

Here it is important to distinguish between trans-Arctic navigation, i.e., transporting cargo between Europe and Asia (and vice

\* Corresponding author.

E-mail addresses: [yka@noc.ac.uk](mailto:yka@noc.ac.uk), [yka@noc.soton.c.uk](mailto:yka@noc.soton.c.uk) (Y. Aksenov), [ekp@noc.ac.uk](mailto:ekp@noc.ac.uk) (E.E. Popova), [axy@noc.ac.uk](mailto:axy@noc.ac.uk) (A. Yool), [agn@noc.ac.uk](mailto:agn@noc.ac.uk) (A.J.G. Nurser), [timothy.williams@nersc.no](mailto:timothy.williams@nersc.no) (T.D. Williams), [laurent.bertino@nersc.no](mailto:laurent.bertino@nersc.no) (L. Bertino), [jon.bergh@nersc.no](mailto:jon.bergh@nersc.no) (J. Bergh).

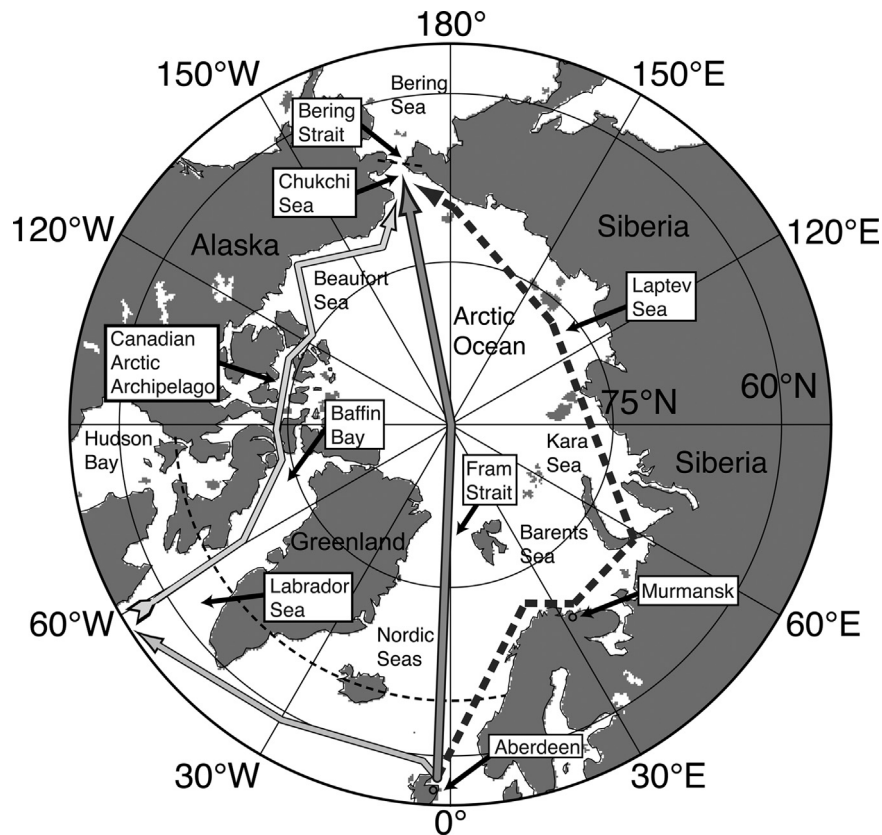


**Fig. 1.** Schematic showing the region of the study. The dashed arrow shows the Northern Sea Route (NSR) along the Siberian Coast from Murmansk (Russia) to Cape Dezhnev in Bering Strait; the light-gray arrow marks the Northwest Passage (NWP) through the Canadian Arctic Archipelago and the Arctic Bridge (AB) from Canada (St. John's, Newfoundland, Canada) to Europe (Aberdeen, UK); the dark-gray arrow shows the North Pole Route (NPR) from Europe (Aberdeen, UK) via Fram Strait across the North Pole to Bering Strait. Thin gray dashed line marks the 65°N boundary of the area used for sea ice analysis.

versa), which is driven by reducing navigational distances, and the regional Arctic shipping of commodities to Arctic settlements and natural resources from the Arctic. The present study addresses the former, whereas the latter has somewhat different economic controls (such as the quantity and type of cargo, commodity prices, vessels draft and accessibility of the few existing ports along the Arctic routes) and as well as social motivation (some of the Arctic settlements are not accessible by roads and can be supplied only by sea [12]). This regional Arctic shipping is beyond the scope of this study. The next section discusses the current state of Arctic shipping and formulates the aims of the present study.

### 1.1. Current state of shipping on the Northern Sea Route

Sailing routes between Europe and East Asian ports through the Arctic Ocean along the Northern Sea Route (NSR) are about 6000 nautical miles (1 nm=1852 m) shorter (43% shorter) than the routes around the Cape of Good Hope and are about 2700 nm shorter (25% shorter) than the Europe to East Asia routes via Suez Canal (Table 1 in [13]). The NSR route is also shorter than the Panama Canal route by about 5380 nm (e.g., [10]). The use of the shipping route across the Arctic to bring cargo from Europe to Asia and vice versa has been explored in the 1990s in a series of international projects [14]. Based on Arctic sea ice and other environmental conditions characteristic of the pre-2000s, the International Northern Sea Route Program (INSROP) estimated that the Arctic shipping route along the NSR could save about 10 days of sailing (a reduction of about 50%) for general cargo type vessels, compared to the shipping route from Asia to Europe via the Suez Canal. The project concluded that savings in sailing time could be achieved if low ice or ice-free conditions were present along the

NSR, although no comprehensive comparison between these two routes was made by the INSROP at that time [15–18]. Schøyen and Bråthen estimated that the NSR reduces the sailing time between Yokohama and London by 44%, as compared to the route via the Suez Canal, if the same average speed is maintained on these two routes [10]. These estimates were later put to the test by practice. For instance, in 2012 a Hong-Kong registered general cargo ship “Yong Sheng” of 14,357 tones of gross register tonnage (GRT) sailed between Dalian (China) and Rotterdam (Netherlands) along the NSR [19]. The ship spent 7.4 days on the NSR, at an average speed of 14.1 knots (1 knot=1 nm per hour) (NSR Information Office, 2015), saving 27% of the sailing time by using the NSR, instead of the route via the Suez Canal (35 days vs. 48 days respectively).

The volume of cargo shipping along the NSR reached its peak in 1987 at 6.6 million tons (331 vessels, 1306 voyages), and then declined in the 1990s and 2000s almost to zero [20,21]. Since the 2000s, the number of cargo-carrying vessels sailing along the NSR has increased again to 71 in 2013, with shipped cargo reaching 1.4 million tons. In 2014 there was a drop in the number of vessels sailing along the NSR to 53. Amongst these, 31 vessels transited on the NSR and 22 vessels were involved in regional supply operations [22]. Data on the volume of cargo in 2014 are not yet available [22].

The shipping data shows a reduction of sailing time along the NSR from 20 days in the 1990s to 11 days on average in 2012–2013. For this calculation the sailing time data is selected from the NSR Information Office database only for transit voyages between the Pacific ports and Europe [22]. The sailing time reduction is attributed to the easier summer ice conditions (ice extent and thickness) in the last decade [12,23].

## 1.2. The aims of the research

Although the Arctic is projected to become seasonally ice-free by the end of the 21st century [24,25], the beginning and the duration of the ice-free season is anticipated to be different for each of the three principal shipping routes across the Arctic Ocean from Europe to the Pacific Asia: (i) the NSR along the Siberian Coast between Murmansk in Russia and Cape Dezhnev in Bering Strait; (ii) the Northwest Passage (NWP) through the Canadian Arctic Archipelago; for the present analysis the NWP is combined with the Arctic Bridge (AB) between Canada (St. John's, Newfoundland, Canada) and Europe (Aberdeen, UK); and (iii) the North Pole Route (NPR) from Europe (Aberdeen, UK) via Fram Strait across the North Pole to Bering Strait (Fig. 1) [13,26,27].

Potential economic and environmental risks in exploiting the NSR lie in the uncertainty of the length of the navigation season, and sudden changes in the oceanic and sea ice regimes in the Arctic [13,28]. One risk is shipping accidents involving oil spills and contamination of the Arctic environment. Changes in the Arctic will also have ecological and socio-economic impacts. Adaptation to the changes requires detailed environmental predictions of the sea ice, ocean, atmosphere and ecosystem.

Since the Rossby radius in the Arctic is less than a few kilometers [29], the ocean circulation features (boundary current and eddies) may also have scales a few kilometers or less, so high-resolution eddy-permitting/resolving ocean models must be used to obtain realistic and detailed ocean simulations. Advanced modeling capabilities are required to quantify spatial and temporal variability of the sea ice in the Arctic, and assess scenarios of the future retreat of Arctic sea ice. This study demonstrates the use of high-resolution ocean and sea ice models for long-term predictions of the future state of the Arctic Ocean, focusing not only on sea ice changes, but also on changes in the ocean circulation, ocean waves and wind. All these are key factors for safe navigation. The aims of the study are two-fold: firstly, to examine the navigability of the Arctic sea routes using a realistic high-resolution detailed future projection of ocean and sea ice conditions, and, secondly, to discuss requirements for sea ice and ocean forecasting models in the changing Arctic.

The paper is structured as follows. The model simulations and analysis methods are described in Section 2. A description of the principal results of the study follows in Section 3 and a more detailed discussion of the findings and directions for future investigation is in Section 4. Section 5 summarizes the study and discusses policy implications, followed by the Glossary and Appendices.

## 2. Data and methods

### 2.1. High-resolution model projections

An eddy-permitting projection of sea ice and ocean state using an Ocean General Circulation Model (OGCM) is used to examine changes in ocean circulation and sea ice cover in the Arctic Ocean in 2000–2099. The model (hereafter, NEMO-ROAM025) is a configuration developed in the Regional Ocean Acidification Modeling project (ROAM) [30]. This is a global high-resolution configuration (nominal horizontal resolution of  $1/4^\circ$  or ca. 28 km, increasing to 9–14 km resolution in the Arctic due to the usage of a tri-polar model grid and model grid convergence) of the coupled sea ice-ocean European model NEMO (Nucleus for European Modeling of the Ocean). The oceanic component of the model Ocean Parallelisé (OPA 9.10) is described in detail in [31]. The sea ice component is the Louvain-la-Neuve sea ice model (LIM2) updated with the Elastic-Viscous-Plastic (EVP) rheology (formalism prescribing

how sea ice cover deforms under external forces) [32,33] and a sea ice thickness distribution in model cells (fractional areas of the cell occupied by sea ice of different thicknesses). The model has been used extensively for oceanographic research, operational seasonal ocean and climate forecasts [34] and climate studies [35]. It is used in operational and climate research modes by a number of operational agencies and centers, such as the UK Meteorological Office (UKMO, UK), Mercator-Océan (France), Metéo France (France), the European Center for Medium Range Weather Forecasting (ECMWF, EU) and Environment Canada (Canada). NEMO is part of the Global Monitoring for Environment and Security (GMES), presently the Copernicus Program, and is used in the Intergovernmental Panel on Climate Change (IPCC) Assessment Reports (AR) as the ocean model component of the CMCC-CM, CNRM-CM5 and IPSL-CM5A(B)-L(M)R climate models [24].

For the present simulation global NEMO-ROAM025 is forced by output from a simulation of the UKMO Hadley Center Global Environment Earth System Model (HadGEM2-ES), run under IPCC Assessment Report 5 (AR5) Representative Concentration Pathways 8.5 baseline (excluding climate policies in capping emissions) scenario, hereafter RCP8.5 [36]. The HadGEM2-ES simulation spans 1860–2099 and included terrestrial and oceanic carbon cycles, atmospheric chemistry and aerosols [37] and is one of an ensemble of runs performed for the Coupled Model Inter-comparison Project 5 (CMIP5) and IPCC AR5 [37,38]. The output frequency of the forcing is monthly for precipitation, which includes rain, snow and runoff, daily for downwelling shortwave and long-wave solar radiation and 6 hourly for the atmospheric boundary layer variables: near surface air temperature, humidity and wind velocities [30]. Turbulent air-sea and air-sea ice fluxes are calculated from the HadGEM2-ES output atmospheric fields using standard bulk formulae for the atmospheric near surface boundary layer [39].

The choice of the high-radiative forcing scenario RCP8.5 was motivated by recent assessment of the current CO<sub>2</sub> emissions [4,40,41], which placed the present-day emission trajectory within the 5–95% range and above the 15-percent centile of the RCP8.5 (on an estimated carbon budget of 34.8–39.3 Gt CO<sub>2</sub> in 2014). This changes RCP8.5 scenario from being an extreme climate impact scenario into a high-likelihood climate change scenario, unless sustained emission mitigation from the largest emitting countries is put in place [41].

The model was integrated in two stages. First, a coarser resolution version of global NEMO-ROAM1 (global nominal horizontal resolution of  $1^\circ$  or 111 km, resolution in the Arctic of 36–56 km) was spun up for the period 1860–1974 to obtain a near-present climate state [42]. Next, this state (ocean and sea ice) was used as the initial condition for high-resolution integrations for the period 1975–2099. Sea ice concentration, thickness and drift, along with ocean currents, temperature and salinity, and near surface air temperature (at a 10-m height), latent and sensible heat fluxes between the atmosphere and underlying surface, and 10 m-height winds were output as 5-day mean fields. The output fields were then averaged, to give monthly, seasonal, annual and decadal means. The NEMO-ROAM1 model has the same resolution as the highest resolution of the CMIP5 models (resolution of  $1-2^\circ$ ) and its results are largely comparable with those from the CMIP5 ensemble [24,30], whereas the NEMO-ROAM025 has a 4-times higher resolution. Both the NEMO-ROAM configurations have vertical resolution almost twice as in the CMIP5 models (75 levels in NEMO vs. 30–40 levels in the CMIP5 models), with 19 levels in the upper 50 m and 25 levels in the upper 100 m. The thickness of the top model layer is  $\sim 1$  m and partial steps in the model bottom topography are used to improve the accuracy of the model approximation of the steep continental slopes. The advantage of the high-resolution NEMO-ROAM025 projections, when compared to

the CMIP5 ensemble, is the more realistic simulations of the ocean currents in the Arctic Ocean and elsewhere because it resolves most of the ocean eddies while “permitting” small eddies, and improves simulations of the Arctic Ocean Boundary Current, a principal conduit of the warm Atlantic water into the Arctic Ocean [29,43]. The high vertical resolution and partial bottom steps also improve simulations of the ocean currents on the continental shelf, which is essential for modeling surface ocean dynamics and sea ice. The model has a non-linear ocean free surface, improving simulations of the sea surface height and changes in sea level. For detailed discussion of the model setup see [42].

The present study also uses the lower resolution projection of NEMO-ROAM1 forced with the same RCP8.5 HadGEM2-ES output described above, and with the IPCC AR5 RCP2.6 low emission stabilization scenario [40,41]; both simulations were run for the period 1860–2099 [30]. The integrations were used to examine changes in the sea ice and ocean under different emission scenarios.

## 2.2. Ship safe speed and sailing times

The approach taken here is to utilize the high-resolution projection described above to provide a quantitative assessment of Arctic accessibility for shipping in the 21st century. In the present study the Arctic Transport Accessibility Model (ATAM) [12,44] is applied to the sea ice fields from the projections with NEMO-ROAM025 to calculate safe ship speed (SS) and sailing time (ST) along the Arctic routes. The method closely follows the papers of [12,44], which are the first published uses of ATAM. The ATAM model assumes sea ice conditions are the primary factor impacting the SS and ST in the Arctic Ocean and employs the concept of Ice Numerals (IN) developed by the Arctic Ice Regime Shipping System (AIRSS) [45] in determining ships’ ability to navigate a sea-ice-covered ocean (Eq. (A.1), Appendix A). The AIRSS algorithm defines IN as a sum of Ice Multipliers (IM) for different ice types weighted by their partial fraction. Ice types are derived from the stage of ice development (sea ice age, Table A1, Appendix A), which is defined from ice thickness [12,44,46]. IM are obtained empirically according to different ship classes, taking into account ice types [45]. If IN is positive, the ice conditions are unlikely to be hazardous, thus navigation is safe and SS can be calculated and sailing times along the chosen route are obtained (Eq. (A.2), Appendix A). If IN is zero or negative, the ice conditions may be dangerous, thus sailing is unsafe and SS is set to zero (Table A2, Appendix A). It should be noted, however, that the IN should be considered only as guidance, and the ultimate decision whether to proceed lies with the ship’s Master [45].

A major simplification in the IM calculations made in this study, as well as in previous studies [12,21,27,44] is that IM depends only on ship classes, concentration of different sea ice types and sea ice thickness, but does not explicitly account for ice roughness (area of ridged ice) and ice decay parameters. The reason for this is that the data on stages of thermal ice decay is not routinely available in sea ice models and has been only recently included in the Los-Alamos CICE sea ice model as an extra prognostic variable [47], and ice roughness is not always included in current sea-ice models. The absence of these parameters from sea-ice models is partly due to the lack of robust observational remotely sensed data that might be used to validate and be assimilated into the sea-ice models, and currently these sea ice parameters are still derived qualitatively from visual observations [44,48].

Summer navigation (defined as from June to October, JJASO) conditions along the NPR in the 21st century are assessed for the following 7 types of cargo vessels currently sailing in the Arctic: Canadian Arctic Categories CAC3 (Polar Class 3, PC3) and CAC4 ice-capable vessels and general cargo vessels Types A–E. Type A

corresponds to moderately ice-strengthened Polar Class 6 (PC6) and Type E is a open water vessel (OW) [12,26,45,49]. The ATAM model is used with monthly mean sea ice thicknesses and concentration fields for the decades 2010–2019 (near future state of the Arctic) and 2030–2039 (medium-term state of the Arctic). The results along the NPR are compared with the SS and ST for the three Arctic routes (NSR, NWP-AB and NPR), as assessed by [12,26]. Since in NEMO-ROAM025 with RCP8.5 forcing the summer Arctic sea ice is very low after the 2050s, a different approach, detailed in the next section, is explored to examine conditions in the Arctic over this period.

## 2.3. Sea ice fragmentation and waves in marginal ice zone

The definition of the Marginal Ice Zone (MIZ) varies between different publications. The approach taken in this study is based on satellite products and considers sea ice covered areas with concentration 0.15–0.80 as MIZ [50].

Information on sea ice cover fragmentation (the two-dimensional distribution of maximum ice floe sizes) is presently not routinely available from forecasts or satellite products. For the MIZ in the Arctic the distribution of maximum ice floe sizes can be parameterized following [51] as an exponential function of the sea ice concentration (Eq. (B.1) and Eq. (B.2), Appendix B). The limitation of this approach is that the parameterization has been developed from the analysis of data from Fram Strait, and so may not represent conditions in the compressed winter ice pack. However, with the decline of sea ice and widening of the MIZ in the Arctic, the winter ice pack will occupy less area and this parameterization should be sufficiently accurate for the present analysis. Since the NEMO-ROAM025 projection does not include ocean waves, a quadratic dependency of significant wave height  $H_w$  on wind speed  $U_{wind}$  is assumed for simplicity:  $H_{w2}/H_{w1} = (U_{wind2}/U_{wind1})^2$ ; indices 1 and 2 refer to wind speed and wave heights at present and in the future, respectively. This allows us to obtain an estimate of the  $H_w$  increase, although this does not account for the wave fetch increase [52]. For short-term forecasting coupled wave and sea-ice models can be used as shown in Section 3.5 [53].

## 3. Results

### 3.1. Verification of the sea ice model

To evaluate the model skills and biases in simulating present Arctic sea ice cover, the simulated spatial distribution of sea ice concentration (fractional area of the ocean covered by ice) along with time series of the pan-Arctic sea ice extent (the area over which ice is present) and volume (product of ice thickness and concentration) are compared with observational datasets. This model evaluation guides the assessment of the projected future sea ice and ocean state.

Observed sea ice concentrations are taken from the UKMO Hadley Centre Sea Ice and Sea Surface Temperature (HadISST1) dataset [54]. The HadISST1 dataset is based on multi-decadal passive microwave satellite remote sensing products of the global sea ice cover from 1978 until present (hereafter 2014). In order to examine model performance in different seasons, monthly simulated and observed sea ice concentration fields are averaged for winter (December–February, DJF), spring (March–May, MAM); summer (June–August, JJA) and autumn (September–November, SON) for 1978–present, thus creating mean seasonal averages for this period.

The realism of the simulated variability and trends in sea ice are assessed by comparing monthly time series of sea ice extent obtained

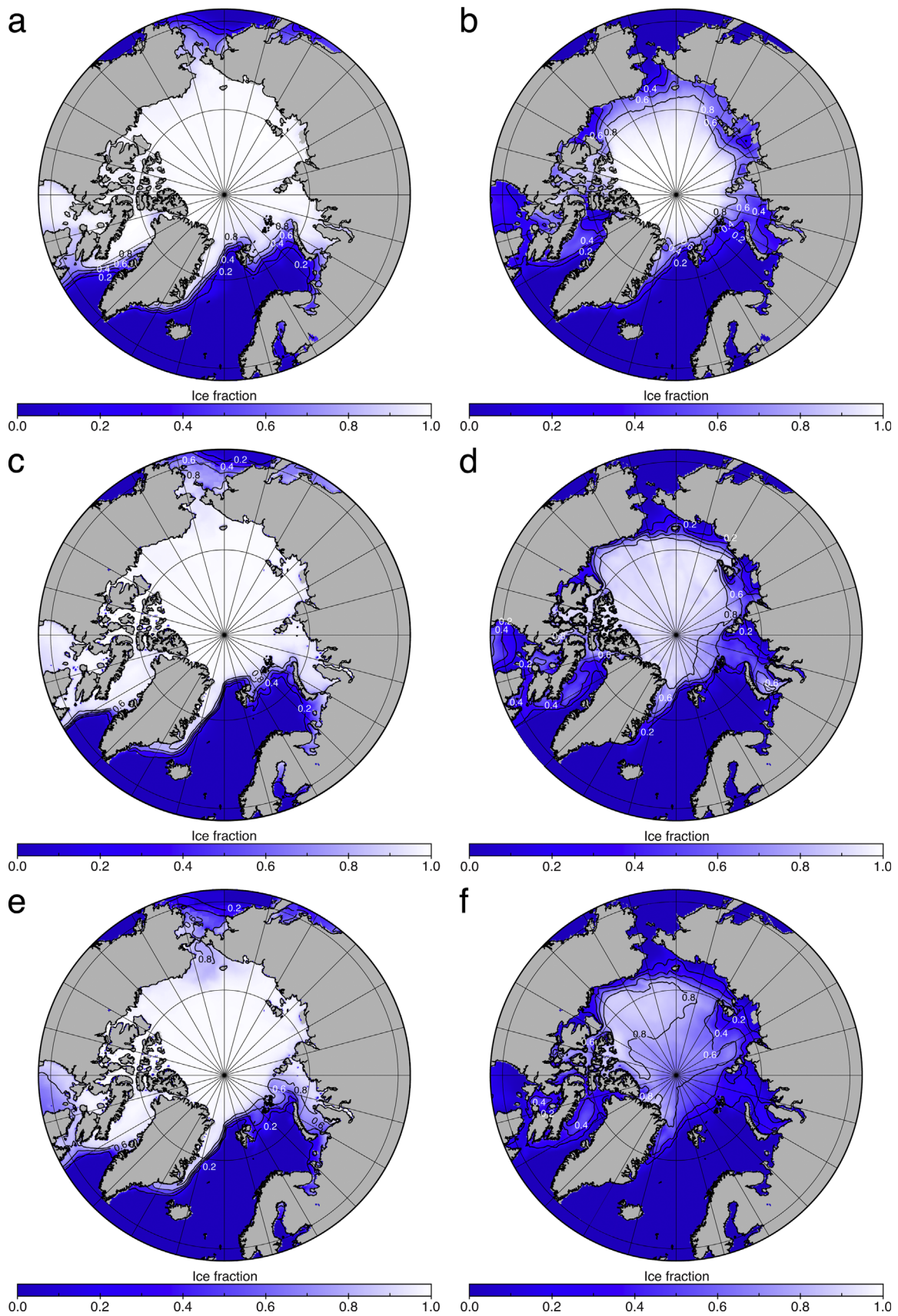


**Fig. 2.** (a,c and e) Mean 1978–2005 winter (December–February) and (b,d and f) summer (June–August) sea ice fraction (shades of blue and contours) from the HadISST1 [54] (a and b) and from the NEMO-ROAM025 model (c and d). (e) Model winter (December–February) and (f) summer (June–August) 2030–2039 ice fraction from the NEMO-ROAM025 RCP8.5 projection (shades of blue and black contours). (For interpretation of the references to color in this figure legend, the reader is referred to the web version of this article.)

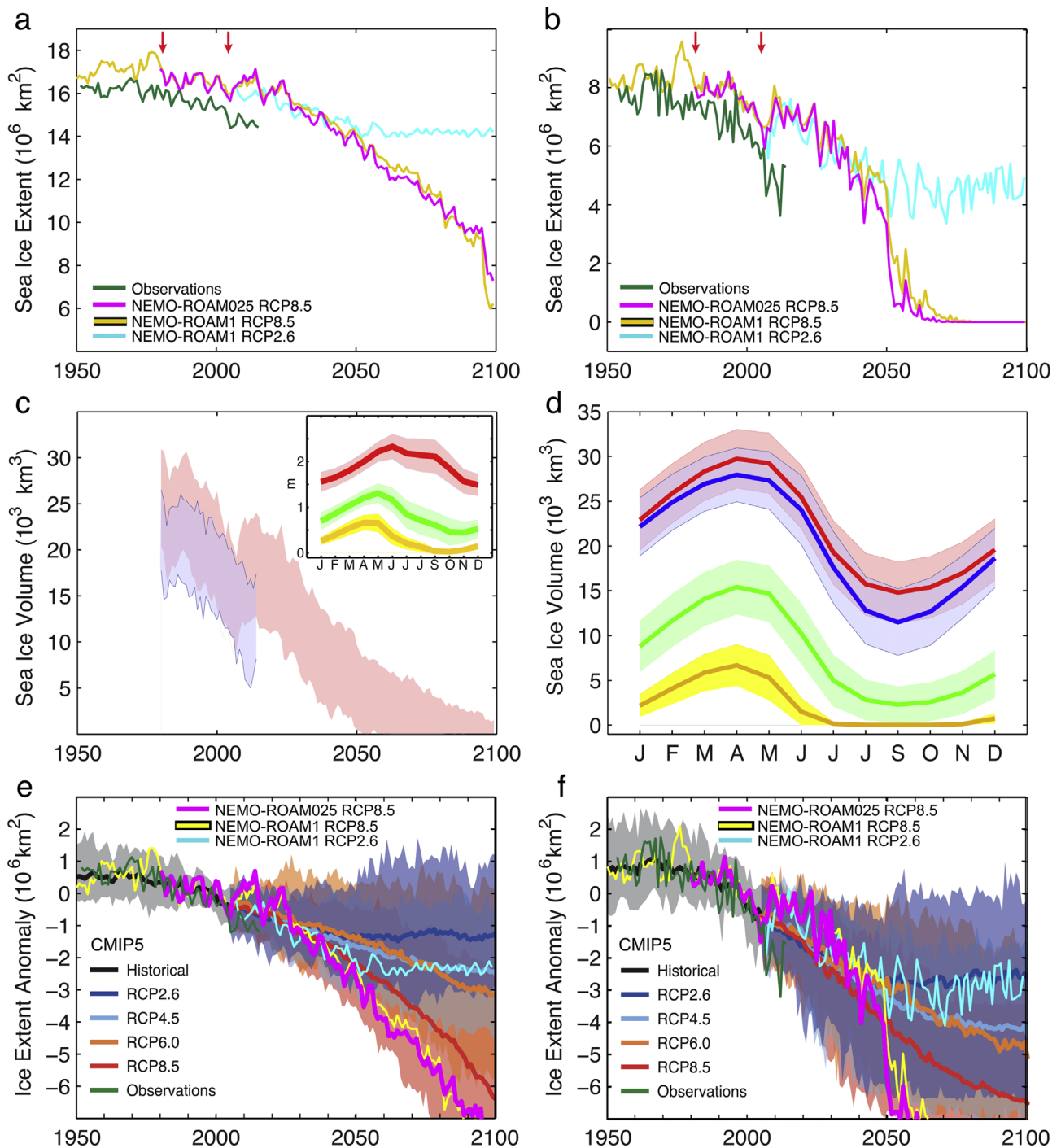


**Fig. 3.** (a) Winter (February) and (b) summer (September) observed sea ice extent 1953–2015 (green line) from NSIDC [61] and HadISST [54] datasets and simulated over 1975–2099 in NEMO-ROAM025 RCP8.5 (magenta), over 1953–2099 in NEMO-ROAM1 RCP8.5 (yellow) and in NEMO-ROAM1 RCP2.6 (light blue). Red arrows show the start of the NEMO-ROAM025 run in 1978 and the end of the historical forcing and beginning of the projected RCP8.5/2.6 forcing in 2005. (c) Monthly ice volume simulated by NEMO-ROAM025 RCP8.5 (red) and from PIOMAS (blue) for 1980–2015. (d) The corresponding modeled seasonal cycle of ice volume (red) and from PIOMAS (blue). Modeled seasonal volumes are also shown for 2030–2059 (green) and 2060–2099 (yellow). The inset in (c) shows the corresponding seasonal cycles of modeled mean ice thicknesses. Solid lines mark means and color shading denotes  $\pm$  one standard deviation. (e) Winter (February) and (f) summer (September) sea ice extent anomaly (relative to the 1986–2005 winter and summer means respectively) in the NEMO-ROAM025 RCP8.5 simulations (magenta) and in the NEMO-ROAM1 simulations forced by RCP8.5 (yellow) and RCP2.6 (light blue). The corresponding sea ice extent anomalies in the CMIP5 ensembles for the different emission scenarios from the IPCC report [37] are shown as solid color lines with shading denoting 5 to 95% of the ensembles. Green lines depict the observed winter and summer sea ice extent anomalies over 1953–2015 obtained from NSIDC and HadISST datasets.

from HadISST1 with those from the model and by comparing simulated sea ice volumes with those from the Pan-Arctic Ice-Ocean Modeling and Assimilation System reanalysis (PIOMAS) [55]. The sea ice extent time series is computed by summing two-dimensional monthly sea ice extent fields for 1978–2013 over the area north of

65°N, including the Arctic Ocean, the Arctic shelf seas and the waters of the Canadian Arctic Archipelago, the Nordic Seas, the Baffin Bay, but excluding the Hudson Strait and Bay, the Labrador and Bering seas (Fig. 1). The simulated volumes are integrated over the area above for 1979–2005 and compared to those from PIOMAS.

The sea ice state for the current climate (1970s–2010s) simulated by NEMO-ROAM025 agrees with data (Figs. 2 and 3). Winter ice fractional concentration (or ice fraction) in the model and data is in good agreement (Fig. 2a and c). In the model there is a moderate underestimation of summer sea ice fraction northeast of Svalbard and an overestimation of ice summer fraction in the Chukchi and East Siberian seas (Fig. 2b and d). The simulated sea ice extent and volume trends are consistent with those currently observed (Fig. 3a–c), although the model overestimates both sea ice extent by about 7% and 15% in the winter and in the summer respectively (Fig. 3a and b) and annual volume by about 15% (Fig. 3c and d).

### 3.2. Changes in sea ice

The NEMO-ROAM025 high-resolution forward projection, forced with the RCP8.5 scenario, and the lower-resolution NEMO-ROAM1 forced by both RCP8.5 and RCP2.6 forcing give a consistent picture of sea ice changes in the 21st century, as compared to the CMIP5 model scenarios (Fig. 3e and f) [24,37]. Both NEMO-ROAM simulations and the corresponding IPCC AR5 RCP8.5 models appear similarly too conservative in predicting currently observed sea ice decline (sea ice reduction in the models is too low) [56–59]. Moreover, there is a little difference in both the sea ice extent and volume between the NEMO-ROAM025 and NEMO-ROAM1 forced forward projections on one hand, and the respective HadGEM2-ES coupled simulations on the other (cf., Fig. 3a–c and Figs. 3 and 4 in [60]). Since the forced and coupled models show a similar sea ice response to the warming, the conservative biases in the projections are not due to the lack of ocean-ice-atmosphere feedbacks, but result from deficiencies in the physical description of the underlying sea ice processes [57,59]. Until the 2050s, NEMO ROAM projections closely follow the CMIP5 RCP8.5 ensemble mean and for the 2060s–2090s are within 5–95% of the CMIP5 ensemble (Fig. 3e and f).

The RCP8.5 scenario presents a substantial increase in global and Arctic surface air temperatures (SAT) and in Arctic sea surface temperature (SST) (Fig. 4). Between the 2000s and 2090s, SST in the Arctic Ocean and Siberian seas increases by about 2 °C in the winter and by about 7 °C in the summer, reaching averaged values of about 2–3 °C and 5–8 °C in the winter and summer respectively (not shown). Similar to the CMIP5 RCP8.5 model ensemble, the model presents conservative simulations for the current sea ice climate (Fig. 3e and f). The NEMO-ROAM1 sea ice simulations with RCP8.5 are similar to those with NEMO-ROAM025, except for the last ten years of the integrations, when ice in NEMO-ROAM025 declines more slowly than in NEMO-ROAM1 in the winter and more rapidly in the summer.

In both runs the shape of the seasonal cycle in sea ice volume does not change with declining ice, although there is a clear reduction in the mean and the amplitude of the cycle (Fig. 3d). The seasonal cycle of mean ice thickness changes: the maximum shifts from June to May and the secondary maximum in September, due to melting of first-year ice, disappears (inset in Fig. 3c). In the model projection, summer ice retreats first in the Eurasian Arctic and in the Siberian seas (Fig. 2) but there are only moderate changes in winter ice extent until the 2030s, falling from 16.2 million km<sup>2</sup> in 2000–2009 to 14.8 million km<sup>2</sup> in 2030–2039 (area fall from 15.4 million km<sup>2</sup> to 14.1 million km<sup>2</sup> respectively) (Fig. 3a). Ice retreats more rapidly from the 2030s with ice extent reaching 8.8 million km<sup>2</sup> (area 7.7 million km<sup>2</sup>) in the Arctic by the 2090s (Fig. 3a).

### 3.3. Changes in ocean circulation

The oceanic geostrophic balance (i.e., lateral pressure gradient

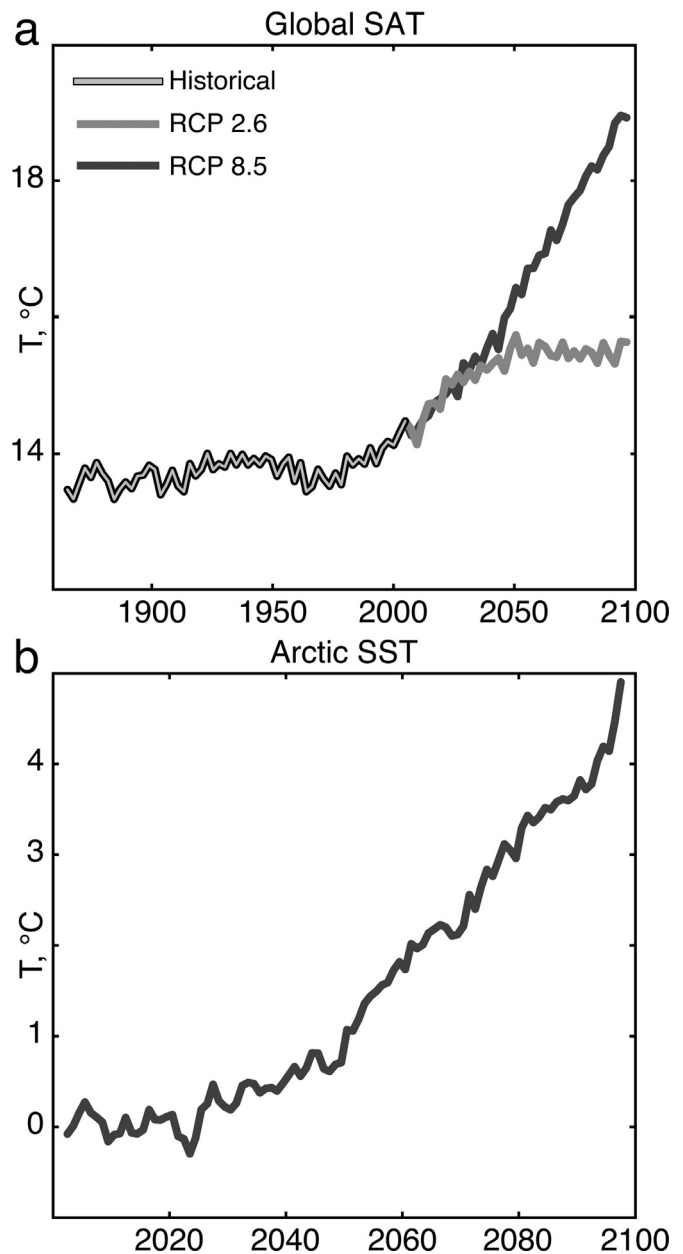
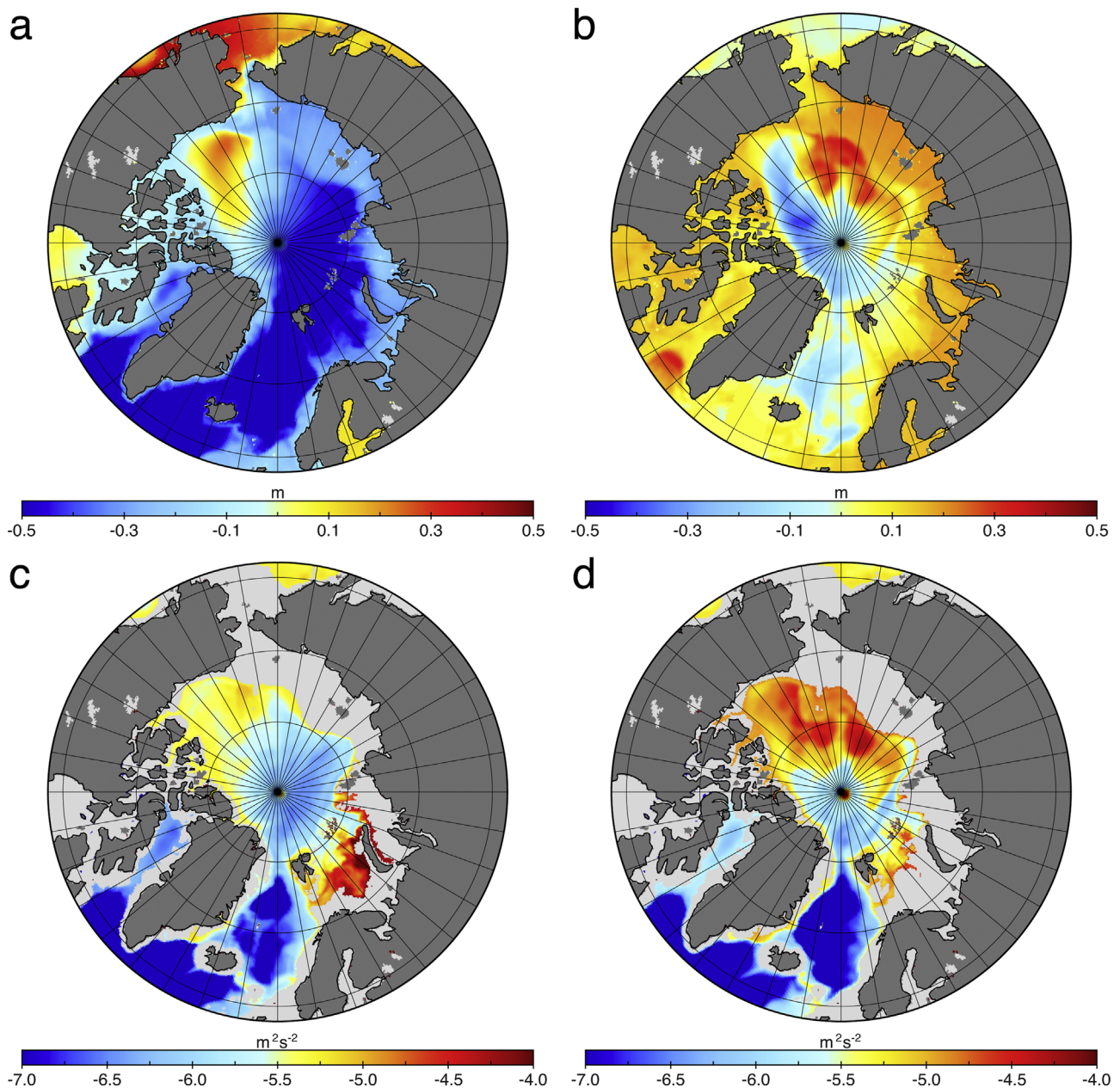


Fig. 4. Timeseries of the global annual mean surface air temperature 1860–2099 in the RCP2.6 and RCP8.5 projected atmospheric forcing (a) and of the pan-Arctic annual mean sea surface temperature 2000–2099 in the RCP8.5 forcing (b).

is balanced by the Coriolis force) holds in the Arctic Ocean for time averages longer than a month, which permits the ocean circulation to be analyzed using the Montgomery function, mapped on pseudo-neutral surfaces [43].

The method allows the use of scalar stream-function-like surfaces instead of the vector fields, and simplifies analysis of the ocean circulation and attribution of driving mechanisms. The present analysis is focused on the effects of wind on the upper ocean dynamics (down to 600 m depth). To examine the changes in the surface ocean currents, two-dimensional fields of sea surface height are analyzed as an approximation of the geostrophic surface circulation.

Like the sea ice, the surface circulation shows a large change after the 2040s. The anti-cyclonic circulation in the Beaufort Sea of the Canadian Basin, a characteristic of the present-day Arctic circulation [62,63], disappears, and a large cyclonic gyre develops in the western Arctic Ocean, with a strong localized anti-cyclonic



**Fig. 5.** Model mean sea surface heights (a) in 2040–2049 and (b) change between 2040–2049 and 2090–2099 from the RCP8.5 NEMO projection (color). Mean 2040–2049 (c) and 2090–2099 (d) Montgomery potential (equivalent of geostrophic stream function) at the 27.8  $kg/m^3$  density surface (about 300–600 m depth) from the same projection (color).

gyre in the East-Siberian Sea and in the eastern Canadian Basin (Fig. 5a and b). The principal driving mechanism is reduction of the high atmospheric sea level pressure (SLP) in the Beaufort Sea and decrease of the Ekman convergence in the Beaufort Gyre [64]. The other feature is the “short-circuiting” of the Arctic surface circulation in the Nordic Seas, resulting in the Arctic surface waters recirculating back in the Arctic Ocean, instead of flowing out into the North Atlantic (Fig. 5a and b). The Montgomery potential shows a change from a weak cyclonic boundary flow to an anti-cyclonic ocean circulation at intermediate (200–600 m) depths in the Canadian Basin after the 2040 s (Fig. 5c and d). This change also results from changes in the atmospheric wind, which increase the high oceanic pressure (high Montgomery potential) in the Central Arctic in the 2090s. The pressure increase acts against the high oceanic pressure present in the Barents Sea before the 2040s and blocks the boundary current emerging northwards from the

Barents Sea (Fig. 5c and d).

### 3.4. Accessibility of summer shipping routes

Following the method described in Section 2.2, the ship safe speed (SS) on the NPR is calculated for the 7 ship classes (CAC3, CAC4, and Types A–E) for the projected averaged summer sea ice conditions in 2010–2019 and 2030–2039. For each model cell Ice Multipliers (IM) and Ice Numerals (IN) are computed (Tables A1 and Table A2, Appendix A). To obtain the corresponding sailing time (ST) on the NPR, the shortest path in the model domain between Aberdeen (UK) and Bering Strait is defined (Fig. 6). In addition, optimized routes to avoid impassable ice type for each of the 7 ship classes are defined via choosing a path through the 2-D IN fields that steps only through the positive IN values and minimizes the distance between the port of departure (Aberdeen, UK) and destination (Bering Strait). All sailing

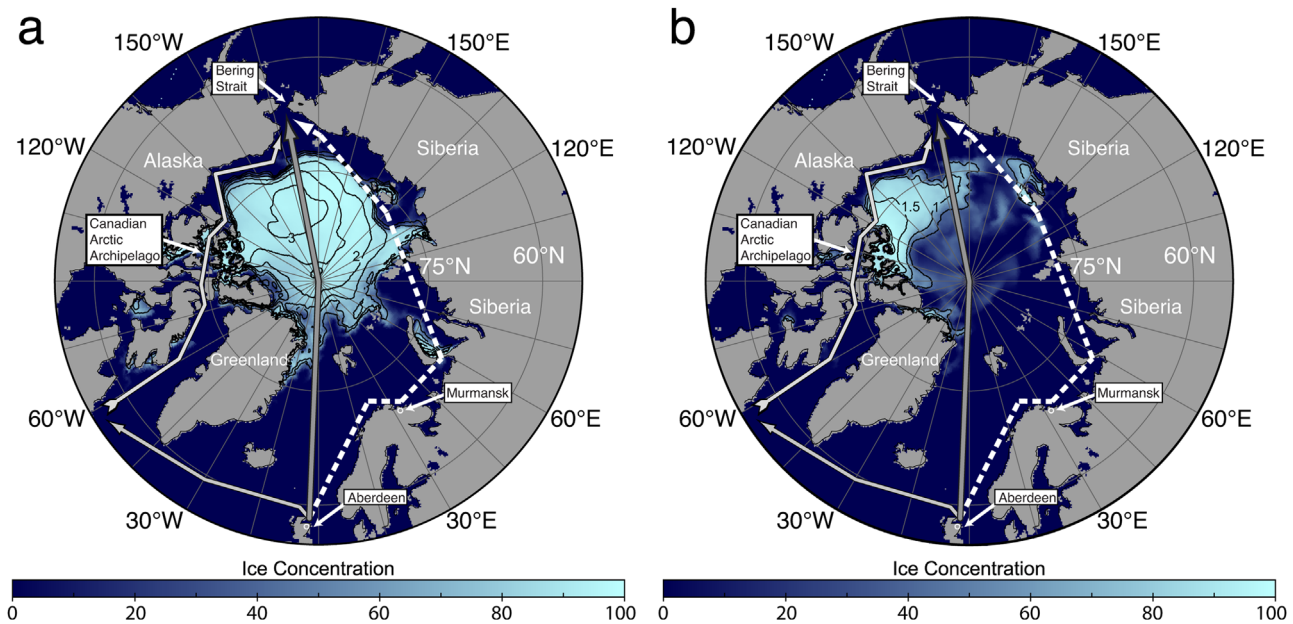


**Fig. 6.** Model 2010–2019 (a) and 2030–2039 (b) sea ice concentration (%; shades of blue) and thickness (labeled contours) during the navigation period (June–October) from the RCP8.5 NEMO projection. The Arctic shipping routes are shown schematically: the Northern Sea Route (NSR) (dashed arrow), the North Pole Route (NPR) (dark-gray arrow) and the Northwest Passage (NWP) and Arctic Bridge (AB) (light-gray arrow).

times are calculated by summing up the times required to cross each of the model cells along a selected route.

In the 2010s, the thick and compact second year ice remains in the Central Arctic on the NPR (Fig. 6a) and the route is inaccessible for Type A–E general cargo vessels. The ice-capable vessels CAC3 (PC3) and CAC4 can navigate the NPR by avoiding areas of thickest ice in the Canadian Basin (Fig. 6a). The sailing time estimates are 16–19 days for these optimized routes (Table 1). To transit the high Arctic, Type A (PC6) vessels have to avoid multi-year and second year pack ice and thick first-year pack ice as well. This pathway takes these vessels far away from the NPR, almost along the NSR (Fig. 6a). Ice conditions are easier on the NSR but the longer distances result in the sailing time of 20 days (Table 1). The less ice-capable Type B–E are unable to safely break compact pack ice thicker than 0.7 m, therefore they cannot transit the Arctic Ocean offshore and must to follow the NSR (Fig. 6a). The inaccessibility of the NPR for general cargo vessels until the end of the 2010s in the present analysis is consistent with the results by Smith and Stephenson [26], who performed Arctic shipping accessibility analysis using the CMIP5 ensemble and concluded that the direct route across the North Pole is closed for PC6 (Type A) and open water OW (Type E) ship classes (Fig. 2 in [26]).

During summer in the 2010s and 2020s sea ice concentration in the Central Arctic is predicted to range from 70% to 100% (the

ocean is covered in close pack ice, very close pack ice and compact pack ice [46]) and, therefore, accessibility of the NPR and navigability on the route should be primarily controlled by the sea ice thickness (ice type) distribution along the route. To examine this, a series of optimized route scenarios with fixed ice concentration and perturbations in the ice thickness fields are assessed. It should be noted that all the calculations presented here assume unescorted sailing. If icebreaker support is used, the NPR can be more accessible for the other classes of vessels.

In the 2030s, a large part of the NPR in summer is either ice-free or is covered in open ice (ice concentration of 40–60% [46] (Fig. 6b) and the four ship classes, CAC3 and 4 and Types A and B can safely access the route (Table 1). For the optimized routes constructed in a similar way as for the 2010s, all general cargo vessels are able to navigate the NPR (Table 1). With average sailing times from 13 to 17 days, navigation via the North Pole can compete with the NSR. The sailing times along the NSR (between Murmansk and Bering Strait) were 11 days on average (ranging from 8 to 19 days) for transit shipping in 2012–13 [21,22] and the projected average summer sailing time is 11 days for Type A vessels in the mid-21st century [12]. Adding two days required to navigate the route Aberdeen–Murmansk, the overall sailing times between Aberdeen and Bering Strait is 13 days along the NSR and 15 days along the NPR for Type A vessels.

The sailing times along the NPR obtained using the sea ice data from the NEMO-ROAM025 projection agree well with those obtained using the ATAM with a subset of the CMIP5 models [12,21,27], e.g., average sailing time on the NPR in the 2040–2050s is 16 days for Type A vessels vs 15 days in the NEMO-ROAM025 analysis (Table 1). This supports the validity of the current approach. Thick sea ice remains in the Canadian Basin in the 2030s and affects navigation along the NWP (Fig. 6), preventing practical operational use of this route at least until the mid-century [12].

After the 2050s, the summer sea ice has a very low extent (less than 1 million km<sup>2</sup>) and thickness (less than 0.2 m) (Fig. 3b and inset in Fig. 3c) and does not affect navigation. All types of vessels considered here can safely navigate the NPR. Since substantial areas of the ice-covered Arctic Ocean are transformed to MIZ, the main factors affecting navigation become distances along the

**Table 1**

Predicted averaged sailing time (ST) in days for different Ship Classes (Arctic Ice Regime Shipping System, 1998) along the NPR for the summers 2010–2019 and 2030–2039; n/s-marks sailing is not safe; numbers in brackets show sailing time for the routes optimized to avoid impassable ice types for different ship classes (Table A1).

Ship class	NPR ST 2010–2019 (days)	NPR ST 2030–2039 (days)
CAC3 (PC3)	n/s (16)	13
CAC4	n/s (19)	13
Type A (PC6)	n/s (20)	15
Type B	n/s (20)	16
Type C	n/s (21)	n/s (16)
Type D	n/s (21)	n/s (17)
Type E (OW)	n/s (21)	n/s (17)
Range	(16–21)	13–16(17)

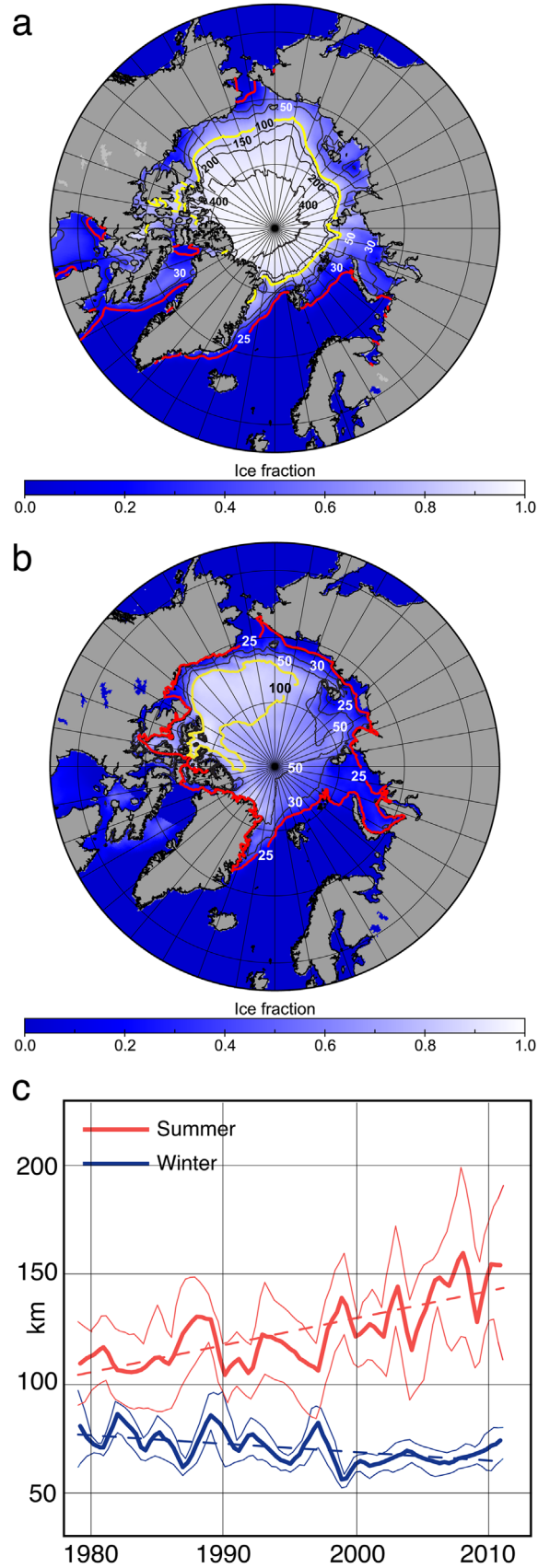


**Fig. 7.** (a) Mean 1978–2005 summer (June–August) sea ice fraction (shades of blue) and mean ice floe sizes in meters (contours with labels). Ice fraction is from the Hadley Center dataset [54]. Red and yellow lines mark the outer (ice fraction of 0.15) and inner (ice fraction of 0.80) boundaries of the MIZ [50]. (b) The same but for 2030–2039 from the NEMO projection. (c) Timeseries 1979–2011 of MIZ width in summer (June–September, red line) and winter (February–April, blue line) from [50]. Means are shown with thick solid lines; thin solid lines show  $\pm$  one standard deviation; and linear trends are marked with dashed lines. (For interpretation of the references to color in this figure legend, the reader is referred to the web version of this article.)

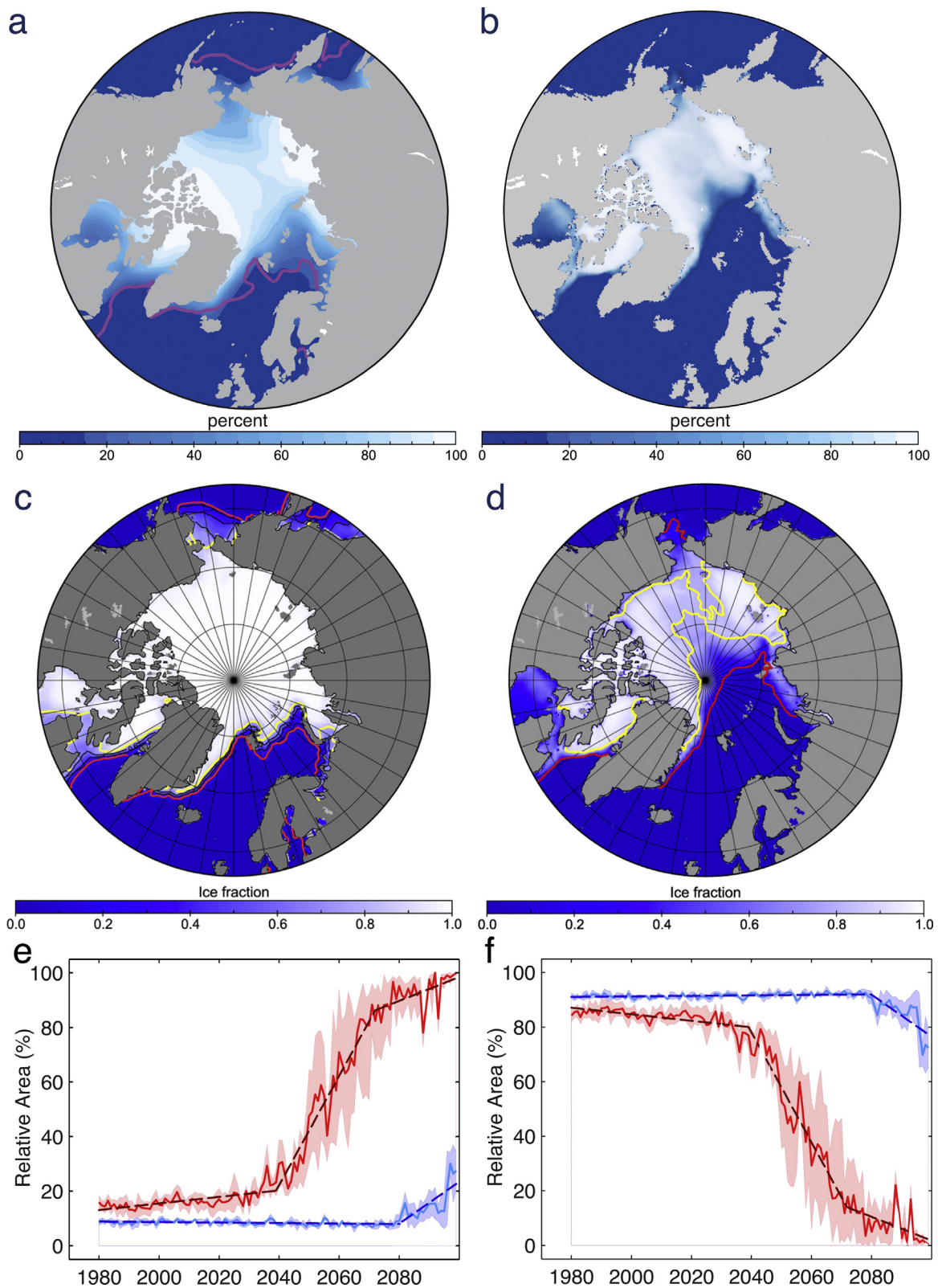


**Fig. 8.** (a) Ensemble mean winter (February) 2080–2099 ice concentration (%), shades of blue) in the CMIP5 models with the RCP8.5 forcing [37] and (b) in the NEMO-ROAM025 projection. Magenta line in (a) shows the 15% isoline of mean February sea ice concentration from 1986–2005 from satellite observations. (c) Mean 2000–2009 winter sea ice fraction (shades of blue) from HadISST1 [54]. (d) The same as (b) but in different shades of blue for easier comparison with (c). Red and yellow lines in (c,d) mark the outer and inner MIZ boundaries. Panels (e) and (f) show the monthly mean (solid) relative area (%) of MIZ (sea ice concentration between 15 and 80%) and of pack ice (sea ice concentration greater than 80%) respectively in winter (December–February; blue lines) and summer (June–August; red lines) from the NEMO-ROAM025 projection. The shading denotes  $\pm$  one standard deviation and dashed lines depict fitted linear trends. (For interpretation of the references to color in this figure legend, the reader is referred to the web version of this article.)

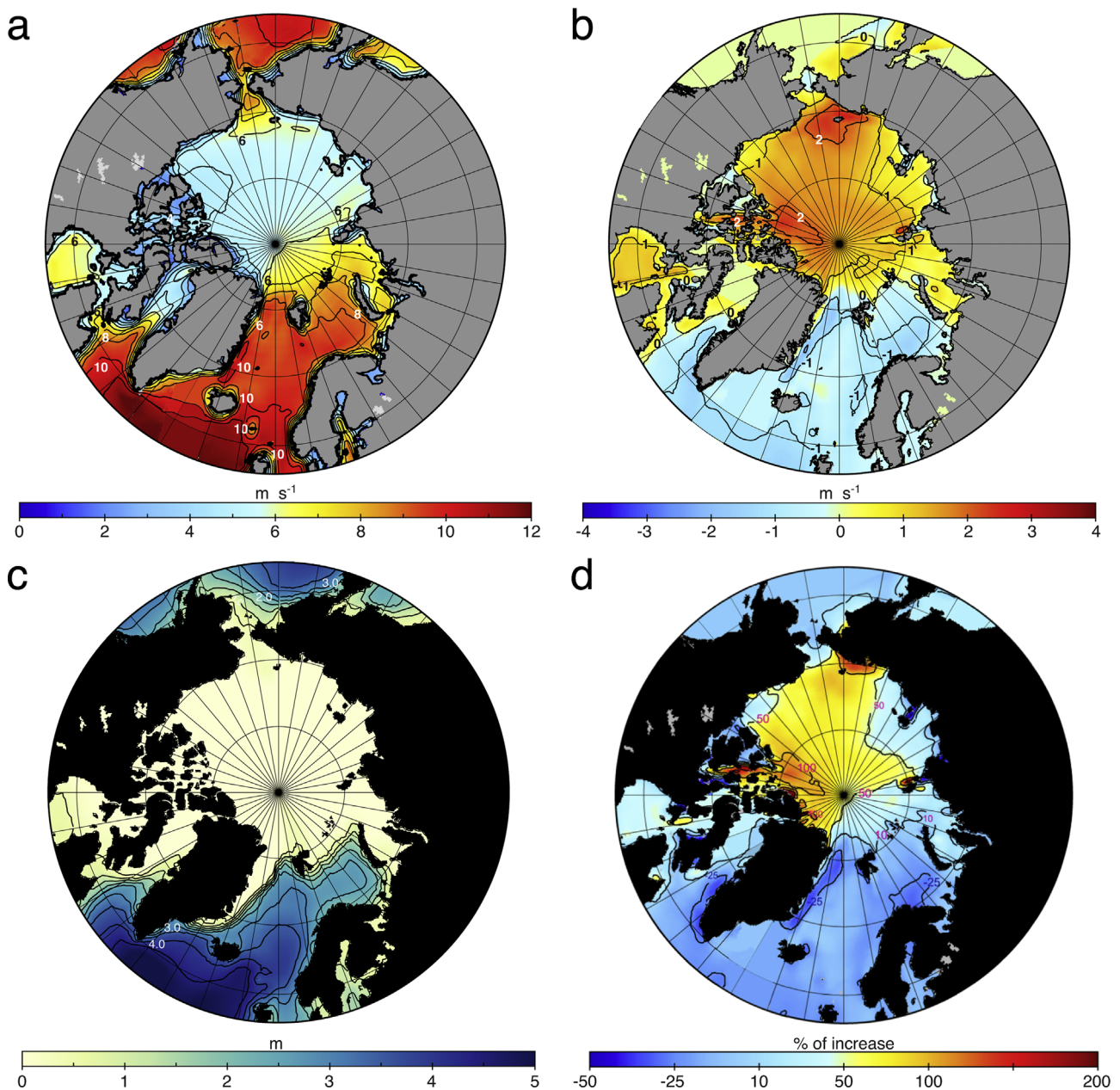


**Fig. 9.** (a) Mean 2000–2009 10-m height mean wind speed over the ocean and (b) corresponding wind speed change between 2000–2009 and 2090–2099 from the RCP8.5 forcing (color and contours). (c) Mean 2000–2009 winter (December–February) significant wave heights (color and contours) from the ECMWF wave model WAM (courtesy Jean Bidlot, ECMWF). (d) Mean 2090–2099 winter (December–February) significant wave height increase in % (color and contours) estimated from 10-m height wind speed change between 2000–2009 and 2090–2099 in the RCP8.5 projection. (For interpretation of the references to color in this figure legend, the reader is referred to the web version of this article.)

route, waves and wind.

### 3.5. Forecasting in the marginal ice zone

Currently the summer Arctic MIZ is widening, reaching on average about 150 km in width [50] (Fig. 7). The NEMO-ROAM025 projection shows a nearly two-fold increase in the MIZ area in summer between the 1978–2005 and 2030s (Figs. 7b and 8). After the 2030s the MIZ percentage in the summer increases from about 20% to about 90% of the total sea ice cover in the 2080s–90s (Fig. 8e). The simulated winter MIZ is about 10% in the 2000s, decreases until the 2080s and then increases again, constituting about 30% of the area of the Arctic sea ice in the 2090s (Fig. 8c–e). With the summer MIZ area increasing, the pack ice (ice fraction greater than 0.8) area in the summer declines in the simulations

and in the 2050s has about the same area as the summer MIZ (Fig. 8e and f). The winter pack ice does not change significantly until the 2090s, when it declines to about 70–80% of total ice area in both the CMIP5 model ensembles (Fig. 8a) and the NEMO-ROAM025 projection (Fig. 8b, d, and f), caused by erosion of the Arctic halocline in summer, making the heat from the Atlantic and Pacific inflows available to melt ice in winter. This is especially noticeable in the Kara and Chukchi seas, where the winter MIZ occupies a significant area (Fig. 8a, b, and d).

Strong and Rigor observed two distinctive tendencies in the summer and winter MIZ width trends during 1978–2011: 39% MIZ widening in summer and 15% narrowing in winter, and explained the winter MIZ decrease by the thermal impact of the North Atlantic water inflow [50]. Although Strong and Rigor examined MIZ width rather than area, their results are qualitatively

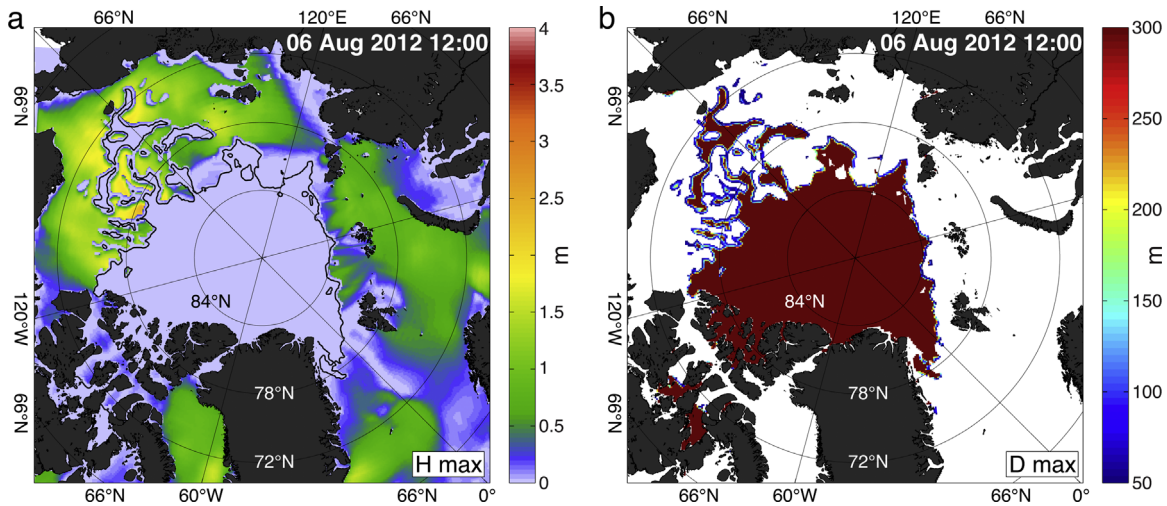


**Fig. 10.** Examples of Arctic wave and ice forecasts with the Towards an Operational Prediction system for the North Atlantic European coastal Zones (TOPAZ): (a) maximum significant wave heights (color) on 6 Aug 2012 12.00 GMT and (b) the same but for maximum ice floe size (<http://topaz.nersc.no/>). Black contour in (a) shows ice edge.

compatible with the MIZ area change in the NEMO-ROAM025 simulation for the same period (Figs. 7c and 8e).

In this emerging state of the Arctic Ocean, when open sea ice cover conditions dominate, sea ice fragmentation (ice floe sizes), wind and waves become the prevailing factors affecting Arctic navigation (e.g., EU Project “Ships and Waves Reaching Polar Regions”, <http://swarp.nersc.no/>). The RCP8.5 forcing demonstrates an increase in winter (DJF) wind speed in the Arctic Ocean by about 50% on average (Fig. 9a and b).

Fig. 9c and d shows that this is accompanied by an increase in significant wave heights in the Arctic Ocean by about 100% on average. (See Section 2.3 for the calculation method). The ice becomes more fragmented, with the maximum ice floe size in the Arctic Ocean decreasing from about 500–1000 m in 1978–2005 to less than 50 m in the 2030s, whereas the floe size in the MIZ decreases to less than 25 m (Fig. 7a and b). With Arctic sea ice shrinking and becoming thinner, the influence of surface waves is stronger. Consequently, a larger part of the sea ice cover acquires dynamic and thermodynamic properties resembling those in the MIZ, rather than the pack ice. These changes require revised approaches to improve the skills of operational simulations and forecasts. Specifically sea ice break-up by the ocean waves and dynamics of the highly fragmented sea ice floes needs to be included in operational modeling [53].

The operational modeling and forecasting system TOPAZ (Towards an Operational Prediction system for the North Atlantic European coastal Zones, see also [65] for details) has taken the above approach and implemented a waves-in-ice module (WIM), which simulates propagation and attenuation of waves into ice-covered areas and mechanical breaking of sea ice floes [53,66,67]. TOPAZ produces experimental forecasts for the North Atlantic and Arctic Ocean at 11–16 km resolution (<http://topaz.nersc.no/>) with a data assimilation component based on the Ensemble Kalman Filter [65]. To demonstrate the effects of surface waves on sea ice break-up and enhanced sea ice melting during strong storm events, the August 2012 storm in the Arctic Ocean has been analyzed in a two-week long simulations using TOPAZ. In August 2012 a strong low-pressure system built up over a few days and generated high amplitude surface waves that were able to travel into the ice-cover and break up the ice into smaller floes (Fig. 10). The area of broken ice was larger on the Pacific side of the Arctic where the storm generated strong waves. This, combined with the long-term thinning and weakening of the sea ice cover led to a rapid sea ice retreat on the Pacific side and to the overall record low sea ice

cover in September 2012.

#### 4. Discussion

Several studies have suggested that Arctic annual surface air temperatures increased by 2–3 °C during the last three decades between 1971–2000 and 2001–2012, with the trends about twice higher than those from the RCP8.5 scenario [68,69]. Therefore, it appears possible that the current emissions in the future may lead to even higher Arctic temperatures than climate model simulations with the RCP8.5 emission scenario predict. This could result in faster sea ice decline in the Arctic than present day climate scenarios suggest, with summer Arctic sea ice disappearance before 2040s [70]. Moreover, with present perennial sea ice reduction of about 20%, the Arctic Ocean has become more vulnerable to a potentially rapid transition toward a seasonally ice-free Arctic state, triggered by natural climate variability [71]. The implications of the rapid Arctic state change for the economies of the Arctic regions are anticipated to be substantial. Along with other industries, the Arctic transport system and maritime industries will have to evolve on a short time scale to adapt to the change and mitigate potential consequences [12,44]. The analysis presented in this study suggests that unescorted navigation in the high Arctic in summer may be possible as early as the 2030–2040s and is probable after the 2050s. The winter seasonal ice in the Arctic will be more fragmented than at present, and its mean thickness will be greatly reduced to about 1 m in the mid 21st century and to about 0.5 m in the second half of the century (Fig. 3d). Winter navigation in the high Arctic most likely will still require support from icebreakers due to highly variable sea ice and ocean conditions in this season.

Stroeve and co-authors analyzed sea ice thickness distribution in the historical CMIP5 ensemble simulations and concluded that, while the basin-scale average sea ice thickness and trends in the Arctic is represented well within the observational uncertainty, spatial patterns of sea ice thickness are poorly simulated [59]. Specifically, the models fail to simulate the thickest ice near the coast of northern Greenland and the Canadian Arctic Archipelago and thinner ice over the Siberian Shelf. This is a critical bias, as the projected ice extent is strongly correlated to the initial ice thickness distribution [59]. It has been shown that ice thickness bias in the Siberian shelf seas is due to absence of a land-fast ice model in the simulations [72,73]; most of the present-day climate models

do not include fast ice physics. On the other hand, the MIZ dynamics is also poorly represented in the climate models [74], which historically use ice rheology developed for compact thick pack ice in the central Arctic [75]. The above and many other examples demonstrate the importance of advanced, physically based sea ice models for accurate predictions of Arctic sea ice evolution and decline. The ice thickness is a key parameter for assessing the navigability of shipping routes and sailing times. Despite advances in satellite technology, sea ice thickness observations are still difficult to make on a routine basis during all seasons [59] and model reanalysis and predictions are still the main source of this vital information.

The simulations presented in this study project a 50% increase in the significant wave height  $H_w$  (Fig. 9). Both observations and the hindcast simulations already show an increase in  $H_w$  in the Arctic Ocean between the 1990s and 2010s, with the average  $H_w$  doubling in the Chukchi and Beaufort Seas [76]. Over this period extreme wave heights have also increased and their recurrence has more than doubled [76]. Thomson and Rogers presented observations of  $H_w$  reaching over 5 m in the Beaufort Sea in September 2012 [52]. This increase in  $H_w$  is attributed to the thinning of sea ice and a longer wave fetch [76]. Since most projections (including the present HaDGEM2 projection) also suggest a significant (50% or more) increase in the wind speed, a larger than a 100% increase in  $H_w$  in the Arctic Ocean in the 21st century is probable [77]. Higher winds and waves, combined with subzero air temperature in the winter, may increase the danger of sea spray deposition on ship superstructures (icing), which has accounted for a substantial number of ship accidents and shipwrecks on the NSR [78]. This poses significant challenges to navigation and offshore exploration, as well as for the ship classification and insurance industries.

Another key result from the simulation is a significant change in the Arctic Ocean circulation, at the surface as well as at depth. By the 2090s the cyclonic flow of the intermediate water in the Canada Basin becomes anti-cyclonic and the boundary current in the Canadian Basin and the Laptev Sea reverses. The changes are similar to those discussed by Karcher and co-workers [79]. In their paper the changes in wind and reduction of sea ice cover were responsible for modification of the momentum transfer from atmosphere to the ocean, leading to an increased anti-cyclonicity in the ocean circulation and reversal of currents. Our forward simulation suggests a potentially complex picture of future Arctic Ocean change, highlighting the importance of high-resolution forecasts and challenging the view that significant changes in the Arctic concern only the sea ice and the atmosphere.

The changes in the Arctic ocean surface and subsurface currents may potentially affect planning of maritime operations in several ways. Firstly, in the absence of sea ice, surface currents become one of the prime factors influencing ship safety, safe speed and sailing times. Secondly, they impact the redistribution of icebergs around Greenland and in the Canadian Arctic Archipelago. Due to a potential “short-circuiting” of the Arctic surface circulation in the Nordic Sea (Fig. 5) some Greenland icebergs may potentially reach Arctic shipping routes. Simulations with an iceberg model coupled to the NEMO OGCM [80] show iceberg spread in the central Arctic Ocean. Lastly, the environmental impact of potential shipping accidents or pollution during the navigation will also depend on ocean currents. The pathways of pollutants can be tracked using high-resolution simulations of ocean currents and sea ice.

## 5. Conclusions and policy implications

According to the simulations, before the 2030s the principal factors for navigation and ship safety are the sea ice conditions. For

long term economic planning, as well as for operational support of navigation and maritime industry, the present transport accessibility models which rely on static information such as sea ice concentration and sea ice types (e.g. ATAM) are adequate in the pack ice areas. However, the acceleration in sea ice drift that has occurred in the last decade requires accounting for sea ice dynamics, i.e., ice drift and ice internal pressure due to sea ice convergence and compression [81]. Marchenko analyzed shipping accidents and shipwrecks on the NSR occurring between the 1930s and 1990s and concluded that ice drift and compression caused about a half of the shipwrecks [78,82], highlighting ice jets (a rapid sea ice flow between drifting and land-fast ice, typically generated by storm surges) as the most dangerous phenomenon for marine transportation in the area.

For more detailed short-term forecasting, a route optimization algorithm is needed to estimate sailing times and accessibility projections should be extended by developing a route optimization tool to estimate the fastest trans-Arctic route given the ice conditions for a particular season and year [26,83]. Additional improvements of the optimal route simulations are envisaged since the present-day coupled atmosphere-ocean general circulation models are continually incorporating more advanced representation of sea ice, ocean and atmospheric physics; amongst these, ice ridging and ice thermal decay affect shipping the most [26].

After the 2030s, when area of pack ice declines and more extensive MIZ-type sea ice provinces emerge, new approaches to forecasting should be considered. The new transport and accessibility models will require more information, including forecasts of winds, currents and waves. More detailed sea ice data will also be required, such as sea ice floe sizes and ice drift parameters. Definitions of sea ice mechanical properties (used for example by oil-rig designers) may need revisiting, as sea ice would be thinner, more saline and weaker [84].

Presently, Arctic exploitation is the center of discussion, weighing mitigation of the consequences of the Arctic changes against potential economic benefits. Therefore there is a little surprise, that after a century of intensive Arctic exploration and more than six decades of using Arctic shipping routes, the economic viability of Arctic shipping is still debated [85]. The challenges are great and lie in balancing economic drivers in Europe, the Americas and in far-eastern countries, such as China, Malaysia, Singapore, Taiwan [86,87], economic risk [85] together with a need for Arctic infrastructure development, with accessible modern ports and roads, etc. [88], and also the impact on the Arctic communities and ecosystems.

Another caveat is that, while the shift of shipping to shorter Arctic routes may decrease fuel use and lower CO<sub>2</sub> emissions, the impact on climate warming may not be wholly negative. This is because the use of Arctic routes may lead to increased concentrations of non-CO<sub>2</sub> gases, aerosols and particles in the Arctic, which can change radiative forcing (e.g. deposition of black carbon on sea ice and snow) and produce more complex regional warming/cooling effects. Simulations of these aspects of Arctic routes suggest that there may actually be a net global warming effect before net cooling takes over [89], thus suggesting that changes in the Arctic maritime use could potentially affect the global economy and global natural environment.

The changes in the Arctic natural environment are occurring faster than elsewhere in the world, and are likely to continue that way for the next few decades together with increased variability of the environmental parameters. They require a system-based approach, combining expertise in different areas, natural and social sciences, engineering, economics, law, policymaking and ecology, capitalizing on the synergy between disciplines. This requires cross-subject international collaboration and close links between

science, engineering and industry. For the shipping industry it is important to initiate cooperation with the forecasting, climate modeling, sea ice, oceanographic and atmospheric observational and modeling communities in order to establish requirements for environmental data and forecasts [23]. This will help assess the potential benefits and risks of Arctic maritime operations and improve their safety.

The present study gives an overview of potential changes in the Arctic relevant to the operation of the sea routes and discusses approaches and challenges in modeling them. The study neither advocates the usage of the Arctic routes, nor presents a complete forecast of the Arctic conditions suitable for detailed shipping planning. Judgment on the former necessitates a comprehensive socio-economic analysis of Arctic navigation, which is beyond the scope of this study, whereas the latter requires further in-depth modeling studies addressing uncertainties in future projections. To the best of the authors' knowledge, this study presents one of the first attempts to combine comprehensive detailed high-resolution environmental information on the future state of sea ice and ocean in the Arctic for practical use by the shipping industry.

The study is linked to several oceanographic initiatives and projects and specifically co-operates with the EU FP7 SWARP Project on introducing ocean wave information and ice break up in the MIZ, as well as with UKMO Earth System Model (ESM) development. With this study the authors have attempted to demonstrate the need for closer interactions between environmental science, engineering and industry in a changing global environment and envisage strong benefits from creating these links.

**Funding for the study**

Drs. Aksenov, Bergh, Bertino, Nurser and Williams acknowledge support from European Union Seventh Framework Programme SWARP (Grant agreement 607476) for this research. Drs. Aksenov, Nurser, Popova and Yool were also funded from the UK Natural Environment Research Council (NERC) Marine Centres' Strategic Research Programme. Dr. Aksenov also was supported from the UK NERC TEA-COSI Research Project (NE/I028947/). The authors are thankful to FAMOS (funded by the National Science Foundation Office of Polar Programs, awards PLR-1313614 and PLR-1203720) for travel support to attend FAMOS meetings. The ocean modeling work in this study was performed as part of the Regional Ocean Acidification Modelling project (ROAM; NERC Grant number NE/H01732/1) and part-funded by the European Union Seventh Framework Programme EURO-BASIN (FP7/2007-2013, ENV.2010.2.2.1-1; Grant agreement 264933). The study used supercomputing facilities provided by the Norwegian Metacenter for Computational Science (Notur). The NEMO-ROAM025 simulations were performed on the ARCHER UK National Supercomputing Service (<http://www.archer.ac.uk>).

**Acknowledgments**

The authors are grateful to Dr. Andrew Coward (NOC) for the help with the global NEMO-ROAM model configuration and Dr. Jean Bidlot (ECMWF) for providing the WAM model data. The authors are also thankful to Prof Kay Riska (Total) for his illuminating talk on the present-day Arctic maritime operations, presented at the Sea Ice Royal Society Meeting in September 2014 and for his comments on the manuscript, to Dr Scott Stephenson (University of Connecticut, CT, USA) for his enthusiasm in discussing industrial and societal consequences of Arctic environmental change, and to Dr Michael Traut (University of Manchester,

UK) for his lecture on the impact of the commercial shipping on Climate, given at the NOC in October 2014 and for the follow up conversations. The waves-in-ice simulation relied on the Norwegian Meteorological Institute (Met Norway) for initial conditions and the Institut français de recherché pour l'exploitation de la mer (Ifremer) for wave information over its duration. The manuscript was also inspired by discussions at the annual Forum for Arctic Modeling and Observing Synthesis (FAMOS) meetings. The authors are also grateful to the anonymous referees for the valuable comments and suggestions, which helped to improve the manuscript. The authors would like to thank the organizers of the Shipping in Changing Climate Conference, which took place in Liverpool in June 2014 under the umbrella of International Business Festival, for providing an excellent opportunity for interaction and discussions between scientists and industry.

**Appendix A. . Calculation of safe ship speed and sailing times**

Following the Arctic Transport Accessibility Model (ATAM) [12,44], the Ice Numerals (IN) are given by:

$$IN = A_{Ni} \times IM_{Ni} + A_G \times IM_G + A_{Gw} \times IM_{Gw} + A_{FY1} \times IM_{FY1} + A_{FY2} \times IM_{FY2} + A_{MFY} \times IM_{MFY} + A_{TFY} \times IM_{TFY} + A_{SY} \times IM_{SY} + A_{MY} \times IM_{MY}, \tag{A.1}$$

where  $A_{Ni,G,GW,\dots,MY}$  and  $IM_{Ni,G,GW,\dots,MY}$  are the sea ice concentration for different Ice Types (IT) and corresponding Ice Multipliers (IM) (Table A1). Ice Types are derived from the mean sea ice thickness in the model cell (Table A1), as it is a good representation of the stage of ice development (ice age), e.g., [90]. From the Ice Numerals, the safe ship speed (SS) is defined for each grid cell on a shipping route (Table A2). The sailing time (ST) is defined by adding the time required to cross all model cells along the

**Table A1**  
Ice Multipliers (IM) for different ice types and ship classes following the Arctic Ice Regime Shipping System (AIRSS) [12,44,45]. Details are in the text.

WMO ice type	WMO ice thickness (cm)	Ship classes						
		Type E (OW)	Type D	Type C	Type B	Type A (PC6)	CAC4	CAC3 (PC3)
MY	300–400	–4	–4	–4	–4	–4	–3	–1
SY	250–300	–4	–4	–4	–4	–3	–2	1
TFY	120–250	–3	–3	–3	–2	–1	1	2
MFY	70–120	–2	–2	–2	–1	1	2	2
FY 2	50–70	–1	–1	–1	1	2	2	2
FY 1	30–50	–1	–1	1	1	2	2	2
GW	15–30	–1	1	1	1	2	2	2
G	10–15	1	2	2	2	2	2	2
Ni	< 10	2	2	2	2	2	2	2

**Table A2**  
Ship safe speed (SS) in nautical miles per hour (nm/h) by Ice Numeral (IN) (Table A1) following the Arctic Ice Regime Shipping System (AIRSS) [12,44,45].

Ice numeral	Safe speed (nm/h)
< 0	0 (Impassable/not safe)
0–8	4
9–13	5
14–15	6
16	7
17	8
18	9
19	10
20	11

route as:

$$ST = \sum_{i=1}^N \frac{D_i}{SS_i}, \quad (\text{A.2})$$

where  $D_i$  and  $SS_i$  are the distances across- and ship safe speed for each model cell.  $D_i$  is calculated as a half of the distance between the central points of two model cells along the chosen sailing track, and there are a total of  $N$  model cells along the sailing track.

## Appendix B. Maximum floe sizes

Maximum sea ice floe size can be empirically related to sea ice concentration as follows [51]:

$$L_i = L_{min} \left( 1 - \frac{A^*}{A} \right)^\beta, \quad (\text{B.1})$$

where  $L_{min}$  is the minimum flow size,  $\beta$  is an exponent to fit the observational data (here  $\beta = 1$ ), and  $A$  and  $A^*$  are the actual and maximum sea ice concentration, where the latter can be written as below:

$$A^* = \left( 1 - \frac{L_{min}}{L_{max}} \right)^{\frac{1}{\beta}}. \quad (\text{B.2})$$

## References

- [1] N. Heitmann, S. Khalilian, Accounting for carbon dioxide emissions from international shipping: burden sharing under different UNFCCC allocation options and regime scenarios, *Mar. Policy* 35 (5) (2011) 682–691, <http://dx.doi.org/10.1016/j.marpol.2011.02.009>.
- [2] K. Anderson, A. Bows, Beyond 'dangerous' climate change: emission scenarios for a new world, *Philos. Trans. R. Soc. A: Math. Phys. Eng. Sci.* 369 (2011) 20–44, <http://dx.doi.org/10.1098/rsta.2010.0290>.
- [3] K. Anderson, A. Bows, Executing a Scharnow turn: reconciling shipping emissions with international commitments on climate change, *Carbon Manag.* 3 (6) (2012) 615–628, <http://dx.doi.org/10.4155/cmt.12.63>.
- [4] A. Bows-Larkin, K. Anderson, S. Mander, M. Traut, C. Walsh, Shipping charts a high carbon course, *Nat. Clim. Chang.* 5 (2015) 293–295, <http://dx.doi.org/10.1038/nclimate2532>.
- [5] Z. Bazari T., Longva, Assessment of IMO mandated energy efficiency measures for international shipping. Estimated CO<sub>2</sub> emissions reduction from introduction of mandatory technical and operational energy efficiency measures for ships Project Final Report, MEPC 63/INF.2, October 31, 2011, International Maritime Organization (IMO), (<http://www.imo.org/en/MediaCentre/HotTopics/Documents/>).
- [6] International Maritime Organization. Reduction of GHG emissions from ships. Third IMO GHG Study 2014 - Executive Summary and Final Report. MEPC 67/INF.3, June 2014 <http://www.imo.org/en/OurWork/Environment/PollutionPrevention/AirPollution/Documents/>. International maritime Organization (IMO), 2014.
- [7] M. Traut, et al., Propulsive power contribution of a kite and a Flettner rotor on selected shipping routes, *Appl. Energy* 113 (2014) 362–372, <http://dx.doi.org/10.1016/j.apenergy.2013.07.026>.
- [8] M.S. Eide, T. Longva, P. Hoffmann, Ø. Endresen, S.B. Dalsøren, Future cost scenarios for reduction of ship CO<sub>2</sub> emissions, *Marit. Policy Manag.* 38 (1) (2011) 11–37, <http://dx.doi.org/10.1080/03088839.2010.533711>.
- [9] M.S. Eide, Ø. Endresen, R. Skjong, T. Longva, S. Alvik, Cost-effectiveness assessment of CO<sub>2</sub> reducing measures in shipping, *Marit. Policy Manag.* 36 (4) (2009) 367–384, <http://dx.doi.org/10.1080/03088830903057031>.
- [10] H. Schøyen, S. Bråthen, The Northern Sea route versus the Suez Canal: cases from bulk shipping, *J. Transp. Geogr.* 19 (4) (2011) 977–983, <http://dx.doi.org/10.1016/j.jtrangeo.2011.03.003>.
- [11] M. Liu, J. Kronbak, The potential economic viability of using the Northern Sea Route (NSR) as an alternative route between Asia and Europe, *J. Transp. Geogr.* 18 (3) (2010) 434–444, <http://dx.doi.org/10.1016/j.jtrangeo.2009.08.004>.
- [12] S.R. Stephenson, L.C. Smith, J.A. Agnew, Divergent long-term trajectories of human access to the Arctic, *Nat. Clim. Chang.* 1 (2011) 156–160, <http://dx.doi.org/10.1038/NCLIMATE1120>.
- [13] A.B. Farré, S.R. Stephenson, L. Chen, M. Czub, Y. Dai, D. Demchev, Y. Efimov, et al., Commercial Arctic shipping through the Northeast Passage: routes, resources, governance, technology, and infrastructure, *Polar Geogr.* 37 (4) (2014) 298–324, <http://dx.doi.org/10.1080/1088937X.2014.965769>.
- [14] R.D. Brubaker, C.L. Ragner, A review of the International Northern Sea Route Program (INSROP)-10 years on, *Polar Geogr.* 33 (1–2) (2010) 15–38, <http://dx.doi.org/10.1080/1088937X.2010.493308>.
- [15] Ø. Andersen T.J. Heggeli T. Wergeland III 10.1: Assessment of Potential Cargo from and to Europe via the NSR. INSROP Working Paper 11-1995. Lysaker: INSROP Secretariat, 1995.
- [16] M. Tamvakis, A. Granberg, E. Gold, *Economy and commercial viability*, in: W. Ostreng (Ed.), *The Natural and Societal Challenges of the Northern Sea Route: A Reference Work*, Kluwer Academic Publishers, Dordrecht/Boston/London, 1999.
- [17] C.L. Ragner Northern Sea Route Cargo Flows and Infrastructure - Present State and Future Potential. FNI Report 13/2000. Lysaker: Fridtjof Nansen Institute; 2000.
- [18] C.L. Ragner, The Northern Sea route-commercial potential, economic significance, and infrastructure requirements, *Post -Sov. Geogr. Econ.* 41 (8) (2000) 541–580, <http://dx.doi.org/10.1080/10889388.2000.10641157>.
- [19] T. Mitchell, R. Milne, Chinese cargo ship sets sail for Arctic short-cut August 11, 2013 *Financ. Times* 2013. August 11, 2013 (<http://www.ft.com>).
- [20] Arctic marine transport workshop (Scott Polar Research Institute, University of Cambridge, in: L.W. Brigham, B. Ellis (Eds.), *Northern Printing, Institute of the North, US Arctic Research Commission, International Arctic Science Committee, Anchorage (AK)*, 2004.
- [21] S.R. Stephenson, L.W. Brigham, L.C. Smith, Marine accessibility along Russia's Northern Sea Route, *Polar Geogr.* 37 (2) (2014) 111–133, <http://dx.doi.org/10.1080/1088937X.2013.845859>.
- [22] North Sea Route Information Office ([http://www.arctic-lio.com/nsr\\_transits/](http://www.arctic-lio.com/nsr_transits/)); 2015.
- [23] T.S. Rogers, et al., Future Arctic marine access: analysis and evaluation of observations, models, and projections of sea ice, *Cryosphere* 7 (2013) 321–332, <http://dx.doi.org/10.5194/tc-7-321-2013>.
- [24] G. Flato, J. Marotzke, B. Abiodun, P. Braconnot, S.C. Chou, W. Collins, P. Cox, F. Driouech, S. Emori, V. Eyring, C. Forest, P. Gleckler, E. Guilyardi, C. Jakob, V. Kattsov, C. Reason, M. Rummukainen, Evaluation of climate models, in: T. F. Stocker, D. Qin, G.K. Plattner, M. Tignor, S.K. Allen, J. Boschung, A. Nauels, Y. Xia, V. Bex, P.M. Midgley (Eds.), *Climate Change 2013: The Physical Science Basis. Contribution of Working Group I to the Fifth Assessment Report of the Intergovernmental Panel on Climate Change*, Cambridge University Press, Cambridge (UK) and New York (NY), 2013.
- [25] D.G. Vaughan, et al., Observations: cryosphere, in: T.F. Stocker, D. Qin, G. K. Plattner, M. Tignor, S.K. Allen, J. Boschung, A. Nauels, Y. Xia, V. Bex, P. M. Midgley (Eds.), *Climate Change 2013: The Physical Science Basis. Contribution of Working Group I to the Fifth Assessment Report of the Intergovernmental Panel on Climate Change*, Cambridge University Press, Cambridge (UK) and New York (NY), 2013.
- [26] L.C. Smith, S.R. Stephenson, New Trans-Arctic shipping routes navigable by midcentury, in: *Proceedings of the National Academy of Sciences*, 2013, 110 (13): E1191–E1195, doi: 10.1073/pnas.1214212110.
- [27] S.R. Stephenson, L.C. Smith, L.W. Brigham, J.A. Agnew, Projected 21st-century changes to Arctic marine access, *Clim. Chang.* 118 (3–4) (2013) 885–899, <http://dx.doi.org/10.1007/s10584-012-0685-0>.
- [28] J. Valkonen, K. Riska, Assessment of the Feasibility of the Arctic Sea Transportation by Using Ship Ice Transit Simulation, in: *Proceedings of the ASME 33rd International Conference on Ocean, Offshore and Arctic Engineering*, American Society of Mechanical Engineers, 2014.
- [29] A.J.G. Nurser, S. Bacon, The Rossby radius in the Arctic Ocean, *Ocean. Sci.* 10 (6) (2014) 967–975, <http://dx.doi.org/10.5194/os-10-967-2014>.
- [30] A. Yool, E.E. Popova, A.C. Coward, Future changes in ocean productivity: is the Arctic the new Atlantic? *J. Geophys. Res.: Ocean.* 120 (11) (2015), <http://dx.doi.org/10.1002/2015JC011167>.
- [31] G. Madec, NEMO team, NEMO ocean engine, version 3.4. Note du Pole de modelisation de l'Institut Pierre-Simon Laplace, No 27 ISSN No 1288–1619, 2012.
- [32] T. Fichefet, M.Á.M. Maqueda, Sensitivity of a global sea ice model to the treatment of ice thermodynamics and dynamics, *J. Geophys. Res.: Ocean.* 102 (C6) (1997) 12609–12646, <http://dx.doi.org/10.1029/97JC00480>.
- [33] S. Bouillon, M.Á.M. Maqueda, Legat V, T. Fichefet, An elastic-viscous-plastic sea ice model formulated on Arakawa B and C grids, *Ocean. Model.* 27 (3) (2009) 174–184, <http://dx.doi.org/10.1016/j.ocemod.2009.01.004>.
- [34] D. Storkey, E.W. Blockley, R. Furner, C. Guivarc'h, D. Lea, M.J. Martin, R. M. Barciela, A. Hines, P. Hyder, J.R. Siddons, Forecasting the ocean state using NEMO: the new FOAM system, *J. Oper. Ocean.* 3 (1) (2010) 3–15, <http://dx.doi.org/10.1080/1755876X.2010.11020109>.
- [35] J.-L. Dufresne, M.-A. Fouchols, S. Denvil, A. Caubel, O. Marti, O. Aumont, Y. Balkanski, et al., Climate change projections using the IPSL-CM5 Earth System Model: from CMIP3 to CMIP5, *Clim. Dyn.* 40 (9–10) (2013) 2123–2165, <http://dx.doi.org/10.1007/s00382-012-1636-1>.
- [36] J. Rogelj, M. Meinshausen, R. Knutti, Global warming under old and new scenarios using IPCC climate sensitivity range estimates, *Nat. Clim. Chang.* 2 (2012) 248–253, <http://dx.doi.org/10.1038/NCLIMATE1385>.
- [37] M. Collins, et al., Long-term climate change: projections, commitments and irreversibility, in: T.F. Stocker, D. Qin, G.K. Plattner, M. Tignor, S.K. Allen, J. Boschung, A. Nauels, Y. Xia, V. Bex, P.M. Midgley (Eds.), *Climate Change 2013: The Physical Science Basis. Contribution of Working Group I to the Fifth Assessment Report of the Intergovernmental Panel on Climate Change*, Cambridge University Press, Cambridge (UK) and New York (NY), 2013.
- [38] C.D. Jones, et al., The HadGEM2-ES implementation of CMIP5 centennial simulations, *Geosci. Model. Dev.* 4 (2011) 543–570, <http://dx.doi.org/10.5194/gmd-4-543-2011>.

- [39] W.G. Large, S.G. Yeager, The global climatology of an interannually varying air-sea flux data set, *Clim. Dyn.* 33 (2–3) (2009) 341–364, <http://dx.doi.org/10.1007/s00382-008-0441-3>.
- [40] P. Friedlingstein, et al., Persistent growth of CO<sub>2</sub> emissions and implications for reaching climate targets, *Nat. Geosci.* 7 (2014) 709–715.
- [41] G.P. Peters, et al., The challenge to keep global warming below 2C, *Nat. Clim. Chang.* 3 (1) (2013) 4–6, <http://dx.doi.org/10.1038/nclimate1783>.
- [42] E.E. Popova, A. Yool, Y. Aksenov, A.C. Coward, T.R. Anderson, Regional variability of acidification in the Arctic: a sea of contrasts. *Biogeosciences*, 11 (2) (2014) 293–308, <http://dx.doi.org/10.5194/bg-11-293-2014>.
- [43] Y. Aksenov, V.V. Ivanov, A.J.G. Nurser, S. Bacon, Polyakov IV, A.C. Coward, A. C. Naveira-Garabato, A. Beszczynska-Moeller, The Arctic circumpolar boundary current, *J. Geophys. Res.: Ocean.* 116 (C9) (2011) C09017, <http://dx.doi.org/10.1029/2010JC006637>.
- [44] S.R. Stephenson, L.C. Smith, J.A. Agnew, Divergent long-term trajectories of human access to the Arctic, *Suppl. Inf. Nat. Clim. Chang.* 1 (3) (2011) 1–28, <http://dx.doi.org/10.1038/NCLIMATE1120>.
- [45] Arctic Ice Regime Shipping System (AIRSS) Standards. Ottawa: Transport Canada; 1998.
- [46] World Meteorological Organization. WMO sea-ice nomenclature: terminology, codes and illustrated glossary. (WMO/OMM/ BMO 259, TP 145, revision Mar 2010). Geneva: World Meteorological Organization, 1970.
- [47] D. Flocco, D. Schroeder, D.L. Feltham, E.C. Hunke, Impact of melt ponds on Arctic sea ice simulations from 1990 to 2007, *J. Geophys. Res.: Ocean.* 117 (C9) (2012) C09032, <http://dx.doi.org/10.1029/2012JC008195>.
- [48] G. Timco, M. Johnston, Arctic Ice Regime Shipping System Pictorial Guide-TP14044, Canadian Hydraulics Institute, Transport Canada, Ottawa, 2003.
- [49] International Association of Classification Societies (IACS), Unified Requirements for Polar Class Ships, Transport Canada, Ottawa, 2009.
- [50] C. Strong, I.G. Rigor, Arctic marginal ice zone trending wider in summer and narrower in winter, *Geophys. Res. Lett.* 40 (18) (2013) 4864–4868, <http://dx.doi.org/10.1002/grl.50928>.
- [51] C. Lüpkes, V.M. Gryanik, J. Hartmann, E.L. Andreas, A parametrization, based on sea ice morphology, of the neutral atmospheric drag coefficients for weather prediction and climate models, *J. Geophys. Res.: Atmos.* 117 (D13) (2012) D13112, <http://dx.doi.org/10.1029/2012JD017630>.
- [52] J. Thomson, W.E. Rogers, Swell and sea in the emerging Arctic Ocean, *Geophys. Res. Lett.* 41 (9) (2014) 3136–3140.
- [53] T.D. Williams, L.G. Bennetts, V.A. Squire, D. Dumont, L. Bertino, Wave-ice interactions in the marginal ice zone. Part 1: theoretical foundations, *Ocean. Model.* 71 (2013) 81–91, <http://dx.doi.org/10.1016/j.ocemod.2013.05.010>.
- [54] N.A. Rayner, D.E. Parker, E.B. Horton, C.K. Folland, L.V. Alexander, D.P. Rowell, E.C. Kent, A. Kaplan, Global analyses of sea surface temperature, sea ice, and night marine air temperature since the late nineteenth century, *J. Geophys. Res.: Ocean.* 108 (D14) (2003) 4407, <http://dx.doi.org/10.1029/2002JD002670>.
- [55] J. Zhang, D.R. Thomas, D.A. Rothrock, R.W. Lindsay, Y. Yu, R. Kwok, Assimilation of ice motion observations and comparisons with submarine ice thickness data, *J. Geophys. Res.: Ocean.* 108 (C6) (2003) 3170, <http://dx.doi.org/10.1029/2001JC001041>.
- [56] J.E. Overland, M. Wang, When will the summer Arctic be nearly sea ice free? *Geophys. Res. Lett.* 40 (2013) 2097–2101, <http://dx.doi.org/10.1002/grl.50316>.
- [57] J.C. Stroeve, V. Kattsov, A. Barrett, M. Serreze, T. Pavlova, M. Holland, W. N. Meier, Trends in Arctic sea ice extent from CMIP5, CMIP3 and observations, *Geophys. Res. Lett.* 39 (2012) L16502-1–7, <http://dx.doi.org/10.1029/2012GL052676>.
- [58] E.D. Malone, et al., North American Climate in CMIP5 experiments: part III: assessment of twenty-first-century projections, *J. Clim.* 27 (6) (2014) 2230–2270, <http://dx.doi.org/10.1175/JCLI-d-13-00273.1>.
- [59] J.C. Stroeve, A. Barrett, M. Serreze, A. Schweiger, Using records from submarine, aircraft and satellites to evaluate climate model simulations of Arctic sea ice thickness. *The Cryosphere*, 8 (5) (2014) 1839–1854, <http://dx.doi.org/10.5194/tc-8-1-2014>.
- [60] P.J. Hezel, T. Fichefet, F. Massonnet, Modeled Arctic sea ice evolution through 2300 in CMIP5 extended RCPs, *Cryosphere* 8 (4) (2014) 1195–1204, <http://dx.doi.org/10.5194/tc-8-1195-2014>.
- [61] J.C. Comiso, F. Nishio, Trends in the sea ice cover using enhanced and compatible AMSR-E, SSM/I, and SMMR data, *J. Geophys. Res.* 113 (C2) (2008) C02S07, <http://dx.doi.org/10.1029/2007JC004257>.
- [62] K.A. Giles, S. Laxon, A.L. Ridout, D.J. Wingham, S. Bacon, Western Arctic Ocean freshwater storage increased by wind driven spin-up of the Beaufort Gyre, *Nat. Geosci.* 5 (2012) 194–197, <http://dx.doi.org/10.1038/NNGEO1379>.
- [63] S.L. Farrell, D.C. McAdoo, S.W. Laxon, H.J. Zwally, D. Yi, A. Ridout, K. Giles, Mean dynamic topography of the Arctic Ocean, *Geophys. Res. Lett.* 39 (L01601) (2012).
- [64] A. Proshutinsky, R. Krishfield, M.L. Timmermans, J. Toole, E. Carmack, F. McLaughlin, W.J. Williams, S. Zimmermann, M. Itoh, K. Shimada, Beaufort Gyre freshwater reservoir: state and variability from observations, *J. Geophys. Res.* 114 (C1) (2009) C00A10, <http://dx.doi.org/10.1029/2008JC005104>.
- [65] P. Sakov, F. Counillon, L. Bertino, K.A. Lisæter, P.R. Oke, A. Korabely, TOPAZ4: an ocean-sea ice data assimilation system for the North Atlantic and Arctic, *Ocean. Sci.* 8 (4) (2012) 633–656, <http://dx.doi.org/10.5194/os-8-633-2012>.
- [66] D. Dumont, A. Kohout, L. Bertino, A wave-based model for the marginal ice zone including a floe breaking parameterization, *J. Geophys. Res.* 116 (C04001) (2011) 1–12, <http://dx.doi.org/10.1029/2010JC006682>.
- [67] V.A. Squire, T.D. Williams, L.G. Bennetts, Better operational forecasting for contemporary Arctic via ocean wave integration, *Int. J. Offshore Polar Eng.* 23 (2) (2013) 81–88.
- [68] M.O. Jeffries, J.E. Overland, D.K. Perovich, The Arctic shifts to a new normal, *Phys. Today* 66 (10) (2013) 35, <http://dx.doi.org/10.1063/PT.3.2147>.
- [69] J.E. Overland, M. Wang, J.E. Walsh, J.C. Stroeve, Future Arctic climate changes: Adaptation and mitigation time scales, *Earth's Future* 2 (2) (2013) 68–74, <http://dx.doi.org/10.1002/2013EF000162>.
- [70] T. Koenigk, Brodeau, R.G. Graversen, J. Karlsson, G. Svensson, M. Tjernström, U. Willén, K. Wyser, Arctic climate change in 21st century CMIP5 simulations with EC-Earth, *Clim. Dyn.* 40 (11–12) (2013) 2719–2743.
- [71] J.C. Stroeve, T. Markus, L. Boisvert, L. Miller, A. Barrett, Changes in Arctic melt season and implications for sea ice loss, *Geophys. Res. Lett.* 41 (2014) 1216–1225, <http://dx.doi.org/10.1002/2013GL058951>.
- [72] M. Johnson, A. Proshutinsky, Y. Aksenov, A.T. Nguyen, R. Lindsay, C. Haas, J. Zhang, N. Diansky, R. Kwok, W. Maslowski, S. Häkkinen, I. Ahik, B. Cuevas, Evaluation of Arctic sea ice thickness simulated by Arctic Ocean Model Intercomparison Project models, *J. Geophys. Res.: Ocean.* 117 (C8) (2012) C00D13, <http://dx.doi.org/10.1029/2011JC007257>.
- [73] M. Janout, Y. Aksenov, J. Hölemann, B. Rabe, U. Schauer, I. Polyakov, S. Bacon, A. Coward, M. Karcher, Y.D. Lenn, H. Kassens, L. Timokhov, Kara Sea freshwater transport through Vilkitsky Strait: variability, forcing, and further pathways from a model and observations, *J. Geophys. Res.: Ocean.* 120 (7) (2015) 4925–4944, <http://dx.doi.org/10.1002/2014JC010635>.
- [74] J. Zhang, A. Schweiger, M. Steele, H. Stern, Sea ice floe size distribution in the marginal ice zone: theory and numerical experiments, *J. Geophys. Res.: Ocean.* 120 (5) (2015) 3484–3498, <http://dx.doi.org/10.1002/2015JC010770>.
- [75] D.L. Feltham, Granular flow in the marginal ice zone, *Philos. Trans. R. Soc. Lond. A: Math. Phys. Eng. Sci.* 363 (1832) (2005) 1677–1700, <http://dx.doi.org/10.1098/rsta.2005.1601>.
- [76] O.P. Francis, G.G. Panteleev, D.E. Atkinson, Ocean wave conditions in the Chukchi Sea from satellite and in situ observations, *Geophys. Res. Lett.* 38 (24) (2011) L24610, <http://dx.doi.org/10.1029/2011GL049839>.
- [77] V.C. Khon, I.I. Mokhov, F.A. Pogarskiy, A. Babanin, K. Dethloff, A. Rinke, H. Matthes, Mokhov II, Pogarskiy FA, Babanin A, Dethloff K, Rinke A, Matthes H. Wave heights in the 21st century Arctic Ocean simulated with a regional climate model, *Geophys. Res. Lett.* 41 (8) (2014) 2956–2961, <http://dx.doi.org/10.1002/2014GL05984>.
- [78] N.A. Marchenko, Russian Arctic Seas. Navigation Conditions and Accidents, Springer-Verlag, Berlin Heidelberg (2012) <http://dx.doi.org/10.1007/978-3-642-22125-5>.
- [79] M. Karcher, J.N. Smith, F. Kauker, R. Gerdes, W.M. Smethie Jr, Recent changes in Arctic Ocean circulation revealed by iodine-129 observations and modeling, *J. Geophys. Res.* 117 (C8) (2012) C08007, <http://dx.doi.org/10.1029/2011JC007513>.
- [80] R. Marsh, V.O. Ivchenko, N. Skliris, S. Alderson, G.R. Bigg, G. Madec, A. Blaker, Y. Aksenov, NEMO-ICB (v1.0): interactive icebergs in the NEMO ocean model globally configured at eddy-permitting resolution, *Geosci. Model. Dev.* 8 (5) (2015) 1547–1562, <http://dx.doi.org/10.5194/gmd-7-5661-2014>.
- [81] S. Somanathan, P. Flynn, J. Szymanski, The northwest passage: a simulation, *Transp. Res. Part A: Policy Pract.* 43 (2) (2009) 127–135, <http://dx.doi.org/10.1016/j.tra.2008.08.001>.
- [82] N.A. Marchenko, Navigation in the Russian Arctic. Sea Ice caused Difficulties and Accidents. Offshore and Arctic Engineering 2013; 32<sup>nd</sup> International Conference on Ocean OMAE 2013, June, France. OMAE2013-10546, doi:10.1115/OMAEE2013-10546.
- [83] V. Kotovirta, R. Jalonen, L. Axell, K. Riska, R. Berglund, A system for route optimization in ice-covered waters, *Cold Reg. Sci. Technol.* 55 (1) (2009) 52–62, <http://dx.doi.org/10.1016/j.coldregions.2008.07.003>.
- [84] T.J.O. Sanderson, *Ice Mechanics and Risks to Offshore Structures*, Kluwer Academic Publishers, Norwell (MA), 1988.
- [85] F. Lasserre, Case studies of shipping along Arctic routes. Analysis and profitability perspectives for the container sector, *Transp. Res. Part A: Policy Pract.* 66 (2014) 144–161, <http://dx.doi.org/10.1016/j.tra.2014.05.005>.
- [86] J. Ho, The implications of Arctic sea ice decline on shipping, *Mar. Policy* 34 (3) (2010) 713–715, <http://dx.doi.org/10.1016/j.marpol.2009.10.009>.
- [87] N. Hong, The melting arctic and its impact on china's maritime transport, *Res. Transp. Econ.* 35 (1) (2012) 50–57, <http://dx.doi.org/10.1016/j.retrec.2011.11.003>.
- [88] B. Noble, S. Ketilson, A. Aitken, G. Poelzer, Strategic environmental assessment opportunities and risks for Arctic offshore energy planning and development, *Mar. Policy* 39 (2013) 296–302, <http://dx.doi.org/10.1016/j.marpol.2012.12.011>.
- [89] J.S. Fuglestedt, et al., Climate penalty for shifting shipping to the Arctic, *Environ. Sci. Technol.* 48 (22) (2014) 13273–13279, <http://dx.doi.org/10.1021/es502379d>.
- [90] J.A. Maslanik, C. Fowler, J. Stroeve, S. Drobot, J. Zwally, D. Yi, W. Emery, A younger, thinner Arctic ice cover: increased potential for rapid, extensive sea-ice loss, *Geophys. Res. Lett.* 34 (24) (2007) L24501, <http://dx.doi.org/10.1029/2007GL032043>.

## Glossary

AIRSS: Arctic Ice Regime Shipping System;

AB: Arctic Bridge;

AR: Assessment Reports;

ATAM: Arctic Transport Accessibility Model;  
CAC: Canadian Arctic Categories;  
CICE: C-ICE Los Alamos sea ice model;  
CMIP5: Coupled Model Intercomparison Project 5;  
ECMWF: European Center for Medium Range Weather Forecasting;  
EEDI: Energy Efficiency Design Index;  
EU: European Union;  
EVP: Elastic–Viscous–Plastic Sea Ice rheology;  
FYI: First-year ice;  
GMES: Global Monitoring for Environment and Security;  
HadGEM2-ES: Hadley Center Global Environment Earth System Model, version 2;  
HadISST1: Hadley Center Sea Ice and Sea Surface Temperature;  
IASC: International Association of Classification Societies;  
IM: Ice Multiplier;  
IMO: International Maritime Organization;  
IN: Ice Numeral;  
INSROP: International Northern Sea Route Program;  
IPCC: Intergovernmental Panel on Climate Change;  
LIM2: Louvain-la-Neuve Sea Ice Model;  
LNG: Liquid Natural Gas;  
MYI: Multi-year ice;  
MIZ: Marginal Ice Zone;  
NEMO: Nucleus for European Modeling of the Ocean framework;  
NPR: Arctic North Pole Route;  
NSR: Northern Sea Route;  
NWP: North-west Passage;  
OGCM: Ocean General Circulation Model;  
OPA: Ocean Parallelisé Model;  
PIOMAS: Pan-Arctic Ice-Ocean Modeling and Assimilation System reanalysis;  
RCP: Representative Concentration Pathways;  
ROAM: Regional Ocean Acidification Modeling;  
SS: Ship Safe Speed;  
ST: Sailing Time;  
SWARP: EU Project “Ships and Waves Reaching Polar Regions”;  
TOPAZ: Towards an Operational Prediction system for the North Atlantic European coastal Zones;  
UKMO: UK Meteorological Office;  
UNFCC: United Nations Framework Convention on Climate Change;  
WIM: Wave in Ice Model;  
WMO: World Meteorological Organization.